OLD DOMINION UNIVERSITY RESEARCH FOUNDATION

DEPARTMENT OF MECHANICAL ENGINEERING AND MECHANICS
SCHOOL OF ENGINEERING
OLD DOMINION UNIVERSITY
NORFOLK, VIRGINIA

SCALE-MODEL STUDIES FOR THE IMPROVEMENT OF FLOW PATTERNS OF A LOW-SPEED TUNNEL

By

P. Stephen Barna, Principal Investigator

Final Report
For the period March 1 - May 31, 1981

Prepared for the
National Aeronautics and Space Administration
Langley Research Center
Hampton, Virginia

Under
Research Grant NSG 1563
Richard A. Margason, Technical Monitor
Low-Speed Aerodynamics Division

January 1982

DEPARTMENT OF MECHANICAL ENGINEERING AND MECHANICS
SCHOOL OF ENGINEERING
OLD DOMINION UNIVERSITY
NORFOLK, VIRGINIA

SCALE-MODEL STUDIES FOR THE IMPROVEMENT OF FLOW PATTERNS OF A LOW-SPEED TUNNEL

By

P. Stephen Barna, Principal Investigator

Final Report
For the period March 1 - May 31, 1981

Prepared for the
National Aeronautics and Space Administration
Langley Research Center
Hampton, Virginia 23665

Under
Research Grant NSG 1563
Richard A. Margason, Technical Monitor
Low-Speed Aerodynamics Division

Submitted by the
Old Dominion University Research Foundation
P.O. Box 6369
Norfolk, Virginia 23508-0369

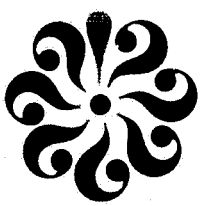

January 1982

TABLE OF CONTENTS

LIST OF FIGURES

FIGURES - CONCLUDED

SCALE-MODEL STUDIES FOR THE IMPROVEMENT OF FLOW PATTERNS OF A LOW-SPEED TUNNEL

By

P.S. Barna*

ABSTRACT

The report summarizes work performed under NASA grant NSG 1563 during the period from March 1 to May 31, 1981. This work was performed on the model V/STOL tunnel housed at Old Dominion University. Significant results were achieved in investigating the following areas:

(1) Static pressure variation around the closed tunnel circuit as affected by the application of various screens;

(2) Pressure rise and radial distribuition of flow through the fan;

(3) Variation of screen parameters and screen location affecting the flow; and

(4) Effects of multiple screens on the velocity distribution in the fourth diffuser.

In these tests the fan was driven through a long shaft by an externally situated 11,190-W (15-HP) motor equipped to turn at 4 speeds.

INTRODUCTION

Studies of the scale-model V/STOL tunnel have been mainly concerned with the velocity distribution observed around the tunnel circuit during the study of 1980. A progress report for the period August 1, 1980 - February 28, 1981 was prepared which contained the main results (ref. 1). While the velocity distributions were found useful for establishing the various flow patterns, they alone did not fully explain the fundamental issues associated with the problems relating to the full-scale tunnel. It was felt that a closer examination was needed which entailed studying the static

*Research Professor, Department of Mechanical Engineering and Mechanics, Old Dominion University, Norfolk, VA 23508.

pressure variations around the circuit, the pressure rise across the fan, and the effects of screens both up- and downstream from their respective points of application.

The static pressure changes around the tunnel circuit help to provide a fair indication of pressure losses due to resistance to flow in the various components, and they also furnish evidence of the pressure gains due to recovery in the diffusers. Although the static pressure rise across the fan (as measured by static tappings) may only be considered an average figure, it may be useful for evaluating the overall effects of the various components on the fan energy demands.

Total pressure changes across the fan blades and their radial locations along the blades furnish details of the fan's performance locally, and from these the overall performance may be obtained by conventional averaging methods. (This method requires a traversing yaw meter.)

Finally, studying flow distribution changes as affected by single or multi-tier screens was deemed of considerable interest and a variety of combinations were tried to discover the most effective screen design.

LIST OF SYMBOLS

A_{geom}	area open to flow as described by the geometry of a duct, m^2
A_{eff}	effective area as defined in Appendix B, m^2
B	blockage, as defined in Appendix B, %
C_{ps}	pressure coefficient relating to static pressure in the tunnel divided by the dynamic head q at test section inlet
d	screen wire diameter, m or cm
m	number of screen wires per unit length
P_s	static pressure at any point of the tunnel circuit, Pa
ΔP_E	Euler pressure rise through the fan
r	radial distance from tunnel centerline (relating to fan), m
R	fan outer radius, m

q	dynamic head, defined as $1/2\ \rho V^2$, Pa
u	velocity of stream at distance y in the various tunnel components as measured from the inner wall, m/s
U_{max}	maximum velocity attained in the stream at any traverse station
V_a	axial velocity of stream downstream from the fan, m/s
V_w	whirl velocity of stream downstream from fan, m/s
V_t	tangential velocity of the fan blades at r distance, m/s
W	width of the tunnel at referenced traverse station, m
y	location of traverse across traverse station measured from inner wall, m
β	porosity of wire screens, percentage defined as $(1 - md)^2$
δ^*	boundary-layer displacement thickness, m
ρ	air density, kg/m^3
ϕ	yaw angle of air velocity downstream from the fan

Abbreviations:

TS	traverse station
H	horizontal traverse
V	vertical traverse
W.G.	water gage

DETAILS OF WORK

Static Pressure Variations

Figure 1(a) is a line diagram of the closed-circuit tunnel while figure 1(b) is a photographic view. The numbers 1 to 21 shown on the line diagram refer to selected traverse stations where velocity distributions were previously obtained (ref. 2) on the full-scale tunnel. In these model tests static pressure tappings were located at relevant points only, particularly near traverse stations 1, 4, 8, 9, 10, 11, 13, 14, 15, 16, 19 and 21. All static pressure was measured relative to atmospheric air, and a nondimensi-

onal, normalized coefficient was obtained by dividing the static pressure, P_s, with the dynamic head, q, measured at TS 21. The pressure coefficient $C_{ps} = p_s/q_{21}$ was then plotted against the tunnel circuit length. The circuit length represented the model by a single straight line as if it were an open tunnel and provided easy recognition of the pressure changes that took place alongside.

The trash screen of the full-scale V/STOL tunnel attached to the turning vanes of the second corner was not simulated in the model tunnel correctly because the presence of the shaft driving the fan prevented its diagonal placement. Instead, it was placed perpendicular to the axis of the tunnel, across the flow at TS 9/B.

A typical set of test results is shown schematically in figure 2 with a screen $m = 42$ and $\beta = 0.59$ at TS 9/B. By "schematically" it is meant that the pressure changes between points are shown as straight lines, which may not be necessarily straight in practice (ref. 3). When inspecting figure 2(a), starting from left, one notices the sharp drop in C_{ps} which was due to the flow acceleration through the contraction between traverse stations 19 and 21. Since the velocity remained essentially constant between TS 21 and TS 1, any further decrease in C_{ps} was mainly caused by skin friction, although a slight acceleration may be anticipated owing to boundary-layer buildup. In the first diffuser (following the test section), recovery between TS 1 and TS 8 appeared quite substantial, indicating that the first diffuser was working satisfactorily. Further downstream, a small drop between TS 8 and TS 9 was experienced due to losses across the corner vanes and flow control vanes. This loss was nearly compensated with the slight recovery in the second diffuser. The trash screen located at TS 9/B, together with the second corner, seemed to cause a considerable drop in C_{ps} between TS 10 and 11, indicating the unduly large resistance to flow caused primarily by the dense screen ($m = 42$, $\beta = 0.59$). The following small rise was due to a modest recovery in the third diffuser upstream from the fan. The rise of static pressure across the fan began at TS 13 just upstream and ended downstream at TS 14 at exit from the counter vanes, where the pressure was found slightly above atmospheric. Some recovery was noticeable in the fourth diffuser between TS 14 and TS 16, up to the location where the air vent was situated. There the absolute pressure was found to

be the highest in the circuit. The slight pressure difference between the inside and atmospheric air allowed the inducted air to be vented outwardly. No substantial pressure changes were found between traverse stations 16 and 19 owing to the very low velocities prevailing there.

Effects of the Air Breather on Pressure

With the air breather open, the pressure dropped and recoveries appeared to be about the same as those with the breather closed. However, the energy expended for inducting the air had to be met by the fan, and the bigger rise in fan pressure indicated the additional energy was needed. Since the air vent set the pressure to be about atmospheric, it also set the pressure at fan exit. To meet this so-called "matching condition," the pressure upstream of the fan must be lower with the air breather open than with it closed. Hence, all pressures between TS 4 (where the air breather is located) and TS 14 must also be lower, as shown in figure 2(b), where for the purpose of comparison pressure variations for both open and closed air breather are plotted.

Effects of Screens on Pressure

Variation of screen parameters appeared to affect the flow both up- and downstream from the screen location. However, the effects downstream are much more marked than those upstream. In figure 3 the pressure variations around the circuit are shown for a variety of setups: without the screen at TS 9/B, as well as with two screens separately applied, one with $m = 42$, $\beta = 0.59$, and the other with $m = 50$, $\beta = 0.32$.

Upstream from TS 8 the pressure appeared to be unaffected; between TS 8 and TS 9, slightly affected; between TS 9 and TS 14, markedly affected; and between TS 14 and TS 18, moderately affected. The application of the low-porosity screen ($\beta = 0.32$) resulted in such a high resistance that the lowest pressure in the circuit fell below $C_{p_s} = -1.2$ and the pressure rise across the fan more than doubled, as compared with the higher porosity and less dense screen ($\beta = 0.59$). Recovery in the third diffuser seemed to improve with screen density, and the rise ΔC_{p_s} between TS 11 and TS 13 was found larger for the low-porosity screen and the smallest for the setup in which no screen was used.

Some of the prototype NASA V/STOL tunnel data are also shown on figure 4, superimposed on data obtained with the model tunnel. It appears that in the full-scale tunnel the pressure drop was smaller in the test section than in the model due to the higher Reynolds numbers. Recovery in the first diffuser seemed to be about equal for both model and prototype; however, the difference becomes more marked between TS 8 and TS 9. The pressure coefficient became more negative in the model, while it remained almost constant in the full-scale tunnel. This means that the losses in the full-scale tunnel when expressed in total head $p_t = p_s + q$ were due to changes in the velocity distribution rather than in changes of static pressure p_s across the corner vanes. The trash screen attached to the third corner in the full-scale tunnel caused a larger drop in pressure due to its lower porosity than that in the model. A geometrically similar screen employed in the model would have caused the same resistance, but at the time of testing a perfectly similar screen was not available for the model experiments*. It appears from figure 3 that the fan automatically compensated for the upstream pressure drop by increasing its pressure rise across the blades. Finally, the small recovery found in the fourth diffuser showed a relatively low efficiency which was partly due to the geometry of the diffuser and was partly caused by the nonuniform velocity distribution at the entrance to the diffuser downstream from the fan. Between traverse stations 16 and 18, changes in the pressure coefficient may be ignored since the dynamic pressure q was small there.

Introduction of various screens at TS 15 increased the load on the fan and markedly improved the velocity distribution at diffuser exit. Among the various experiments performed, there was one combination of screens in which no trash screen was employed upstream of the fan, while at TS 15 (halfway along the fourth diffuser) a single-layer, medium-porosity screen ($m = 24$, $\beta = 0.57$) was installed. Upstream, between traverse stations 8 and 11, the inlet and outlet pressures were found to be about the same; of course, pressure variation between 8 and 11 may be noticeable, but the pressure decreases were compensated by recoveries. However, the pressure rise across the fan increased, thus compensating for the $\Delta C_{p_s} = 0.1$ drop across the screen at TS 15, as shown in figure 4(a). When using a higher porosity ($m = 4$, $\beta = 0.83$) rather coarse trash screen at TS 9/B, and also a higher

---

*For the prototype V/STOL tunnel trash screen, $m \cong 2$, $\beta \cong 0.52$.

porosity (m = 16, β = 0.73) screen at TS 15, a much less severe pressure drop ΔC_{ps} = 0.01 was experienced at TS 15, as shown on figure 4(b).

The experiments with various size orifice plates (17-, 18- and 19-in. diameter openings) upstream from the fan resulted in a pressure decrease upstream of the fan in the third diffuser, where pressure recovery was experienced in tests previously performed without an orifice. To compensate for this drop, the pressure rise across the fan increased, as shown in figure 5. The orifice with the optimum opening of 45.7 cm (18 in.) did improve the fan performance to a limited extent, as will be shown later.

A combination of screens with different mesh sizes and porosities denoted as "composite screens" resulted in markedly improved velocity distribution at the expense of only moderate losses. Several composite combinations were tried, and their respective compositions are shown in Appendix A. Composite A (fig. 6) and composite E (fig. 7) demonstrate pressure variations around the tunnel circuit.

Pressure Rise Across the Fan

Recent studies on diffuser performance clearly established that diffuser performance not only depends on the geometry but also on the velocity distribution at entry (or inlet) to the diffuser. Diffusers with uniform velocity distribution at inlet are claimed to yield high recovery even when the enclosed diffuser angle 2θ is wider than the recommended optimum, thought to be between 5 and 7 degrees (ref. 4). On the other hand, nonuniform velocity distribution affects the performance adversely, and diffusers with high blockage at inlet are known to stall even when their angle is low. It then stands to reason that, if an axial flow fan is situated at diffuser entry, the radial velocity distribution must have a marked effect on the diffuser performance. Such is then the case with the design in the V/STOL tunnel, where the fan is located right at the inlet to the fourth diffuser. Now, in order to establish the "blockage," the axial velocity distribution must be determined. (See Appendix B.)

The performance of the axial flow fan itself can be more fully studied from the contribution to pressure rise of the individual elements that make up the blades. The overall static pressure rise across the fan is generally obtained from the difference in static pressures measured with static

portholes located up- and downstream of the fan. However, such an overall pressure rise may only be considered an approximate average because the radial variation of such quantilities as the whirl and axial velocities, yaw angle, etc. remain unaccounted. To account for these quantities, it is necessary to obtain their radial distribution by established traversing techniques employing yaw probes.

The axial flow fan for the model tunnel was designed for a constant pressure rise along the blade assuming constant axial velocity distribution and "free whirl" (ref. 5). The results of fan tests show that the design assumptions were not fully met in practice, probably because of flow distortions upstream.

In figure 8 through 12, the radial variation of whirl velocity V_w, axial velocity V_a, flow angle downstream from the fan ϕ, and the local pressure rise (Euler "head") Δp_E are plotted against nondimensional radial location, r/R.

Results obtained in absence of upstream screens and orifices are shown in figure 8, where certain peculiarities may be observed which are more or less common to all fan test results, inasmuch as two distinct regions appear: Region I extends between r/R = 0.4 and 0.8, and region II extends between r/R = 0.8 and 1.0. Inside region I the pressure rise was constant, on the average, while the whirl closely followed the free-whirl distribution. While the axial velocity "ran ahead" near the root of the blade, owing to the presence of the elliptically shaped hub, it almost remained constant between r/R = 0.2 and 0.85. Unlike Region I, inside region II all variables, except V_a, began to increase rapidly with increasing radius while V_a decreased rapidly.

Similar results were observed with the application of orifices, as shown in figures 9(a), 9(b), and 9(c). With decreasing orifice size, Δp_E became smaller and the axial velocity was affected to a large extent near the root region, while in the tip region V_a decreased less and less.

With the application of screens upstream of the fan, the flow became more markedly affected as screen density increased and porosity decreased. The axial velocity decreased and the pressure rise across the fan increased in the tip region. Applying a screen at TS 9/B with m = 42 and β = 0.59

resulted in a tip Δp_E = 13.4 in. W.G., as shown in figure 10(a), while a denser screen with m = 50 and low porosity β = 0.32 produced more than 16 in. W.G. tip pressure rise, as shown in figure 10(b). A considerable departure from the ideal free whirl distribution was also observed.

The most peculiar distribution of variables may be seen in figure 11, which shows results with the 43.2-cm (17-in.) orifice in combination with the m = 50, β = 0.32 screen at TS 9/B. Due to a probable flow reversal upstream, the axial velocity fell back near the root (r/R = 0.4 to 0.55), while it remained nearly constant between r/R = 0.55 and 1.0. Also, V_w and Δp_E followed the pattern of V_a near the root and, as before, these markedly increased near the tip.

Application of a screen downstream from the fan did not change the flow across the blades a great deal, as shown in figure 12, where the curves compare favorably with those of figure 8.

SCREEN EFFECTS ON FLOW DOWNSTREAM FROM FAN

Screens at TS 15

The various screens applied at TS 15 (i.e., halfway down the fourth diffuser) produced results which affected the flow distribution mostly downstream. Depending on flow parameters, a single screen located at TS 15 improved the flow at TS 16, as shown in figure 13, where the velocity distributions for two screens, one with m = 24, β = 0.57 and the other with m = 16, β = 0.73, are plotted. When compared with results obtained without a screen, the more dense screen produced a velocity distribution that varied between 1.0 and 0.86. This was a favorable improvement over the no screen distribution, with a variation between 1.0 and 0.67.

Multiple screens with varied porosity applied at TS 15 produced a variety of results, as shown in figure 14. The relevant details of composition of the various screens are shown in figures 14(a) to (e). When comparing the velocity distributions probably the most favorable results were obtained with composite D [fig. 14(d)], where three screens were superimposed. First, a coarse m = 8 base screen was stretched right across the entire flow; at about 20 percent of the width inboard from each side, a second

screen was superimposed with m = 16 and β = 0.73. A center hole of 12.7-cm (5-in.) diameter was cut out of both screens, and a coarse screen with m = 4, β = 0.83 was placed into the cutout. The resulting distribution at TS 16 was almost constant, varying only between 1 and 0.9 across the flow as shown in figure 14(d). The flow distribution shown in figure 14(e) is the result of four tiers, and more humps and hollows may be observed than in figure 14(d). The resulting flow at TS 19 appears about the same in both figures 14(d) and (e), as shown in both graphs superimposesd over the distribution at TS 16. However, since figure 14(d) is a simpler composition than figure 14(e), it demonstrates the distribution more clearly.

Results obtained with higher porosity screens, as shown in figures 14(a), 14(b), and 14(c), where the velocity defects found between V/V_{max} = 0.7 and 1.0 were only marginal improvements.

Screens at Various Traverse Stations

The placing of different single screens (in succession) at TS 9/B indicated the immediate effect of screens close up- and downstream from the screen location. In figure 15 the upstream effects on the velocity distribution are shown superimposed as affected by one screen with m = 42, β = 0.59 and another with m = 50 and β = 0.32. The differences were practically negligible. The downstream effects, however, were quite dramatic, inasmuch as the denser screen (β = 0.32) caused a velocity inversion while the less dense screen (β = 0.59) lifted the low-velocity region, as shown in figure 16. It would be of considerable interest to find that particular screen which would straighten the flow out and render it completely uniform.

The placing of different single screens at TS 9/B also affected the flow immediately ahead of the fan. In figure 17 the results of four velocity traverses obtained at TS 13 with different screens are superimposed. These traverses extended only between the outer wall and the drive shaft because access was blocked by the inner wall.

The results showed similar velocity distributions for three medium-density screens (of which one was a partial) and steadily falling velocities with increasing radii. The dense screen (m = 50, β = 0.32), however, showed a markedly different distribution characterized by a large defect near the

middle (r/R = 0.4) between two peaks, as shown by the solid line on figure 17.

CONCLUSIONS

The experiments performed on the return circuit model tunnel have been divided into three categories: namely, pressure variation around the tunnel circuit, pressure rise across the fan, and velocity distribution across the flow at relevant traverse stations. The tests showed that an interdependence between these categories existed when the resistance to flow was manipulated. Accordingly, the conclusions are as follows:

(1) The results on the pressure variation around the circuit clearly indicated that pressure losses caused by the introduction of screens at any location were accompanied by an increase of overall rise in pressure across the fan, above the rise experienced without the presence of screens. Similar observations were made with the different orifices introduced upstream from the fan.

(2) To compensate for increasing tunnel resistance, the required pressure rise across the fan was affected, and marked changes in radial distribution of the rise have been observed. The tendency was always towards an increase of tip loading, which in turn demanded higher lift at the expense of flow through the tip region. The higher lift was accompanied by higher drag. Thus, the increase of resistance in the circuit was always accompanied by higher blockage, a clearly undesirable flow distribution into the fourth diffuser.

(3) Velocity traverses were also affected by the screens, and the dense screens inverted the velocity field downstream while hardly affecting the flow distribution upstream. The application of various screens upstream did not improve the flow into the fan because the screens, even if they did improve the flow, added resistance which in turn adversely affected the pressure rise across the fan. However, the various combination of screens applied downstream from the fan at TS 15 markedly improved the flow at the fourth diffuser exit without unduly distribing the fan performance.

APPENDIX A

MULTI-TIER SCREEN COMPOSITION

In the multi-tier screens, the base screen designated as "a" stretches from wall to wall right across traverse station 15. Subsequent layers are fastened to the base layer, and their size varies as shown in detail in figure 14 for the five compositions tested. The mesh size m and porosity β are given in the table for each composition:

Composite Designation	Screen Section (Layer) Designation			
	a	b	c	d
A	m = 8	16	8	-
	β = 0.74	0.73	0.74	-
B	m = 8	16	8 (45°)	-
	β = 0.74	0.73	0.74	-
C	m = 8	4	-	-
	β = 0.74	0.83	-	-
D	m = 8	16	4	-
	β = 0.74	0.73	0.83	-
E	m = 8	4	4	2
	β = 0.74	0.83	0.83	0.93

APPENDIX B

CALCULATION OF BLOCKAGE AT ENTRANCE TO LEADING DIFFUSER FROM EXPERIMENTALLY OBTAINED VELOCITY DISTRIBUTIONS

Let blockage

$$B = \frac{A_{geom} - A_{eff}}{A_{geom}}$$

where $A_{geom} = \pi R^2$ and $A_{eff} = A_{geom} - 2\pi R\delta^*$, δ^* being the displacement thickness of the boundary layer. For axisymmetric flow (See fig. B1):

$$U_c 2\pi R\delta^* = \int_o^R (U_c - u)\, 2\pi r dr$$

Introducing $r = R - y$, $dr = -dy$

$$\frac{\delta^*}{R} = \int_1^o \left(1 - \frac{u}{U_c}\right)\left(1 - \frac{y}{R}\right) d\left(\frac{y}{R}\right)$$

For the measured velocity distribution $u = f(y)$, the quantity $\left(1 - \frac{u}{U_c}\right)\left(1 - \frac{y}{R}\right)$ can be plotted against $\frac{y}{R}$ and integrated giving an area, say, A. Hence $\delta^* = AR$ and $B = 2\pi R\delta^* = 2\pi R^2 A$. However, since blockage is expressed in percentage:

$$B\% = \frac{B}{\pi R^2} = 2A$$

Therefore,

$$B\% = 2\int_o^1 \left(1 - \frac{u}{U_c}\right)\left(1 - \frac{y}{R}\right) d\left(\frac{y}{R}\right)$$

Similar considerations apply to the fan annulus at the entrance to the fourth diffuser of the V/STOL tunnel. The blockage can be calculated with the velocity distribution obtained from yaw traverses downstream from the fan between the tip radius R and hub radius R_o. Since the center of the ducting is occupied by a centerbody, U_c may be replaced by U_{max}, which is found near the hub. To obtain the displacement thickness, calculate

$$2\pi R\, U_{max}\, \delta^* = \int_R^R (U_{max} - u)\, 2\pi r\, dr$$

hence

$$\frac{\delta^*}{R} = \int_{R_o}^{R} (1 - u/U_{max})\, \frac{r}{R}\, \frac{dr}{R} = A$$

Since the geometric area $A_{geom} = \pi\,(R^2 - R_o^2) = \pi\, R^2[1 - (R_o/R)^2]$, one obtains the blockage

$$B = \frac{2A}{1 - (R_o/R)^2}$$

Example:

As an example for the axial velocity distribution shown in figure 10(a) on page 30, one obtains a blockage of 20 percent.

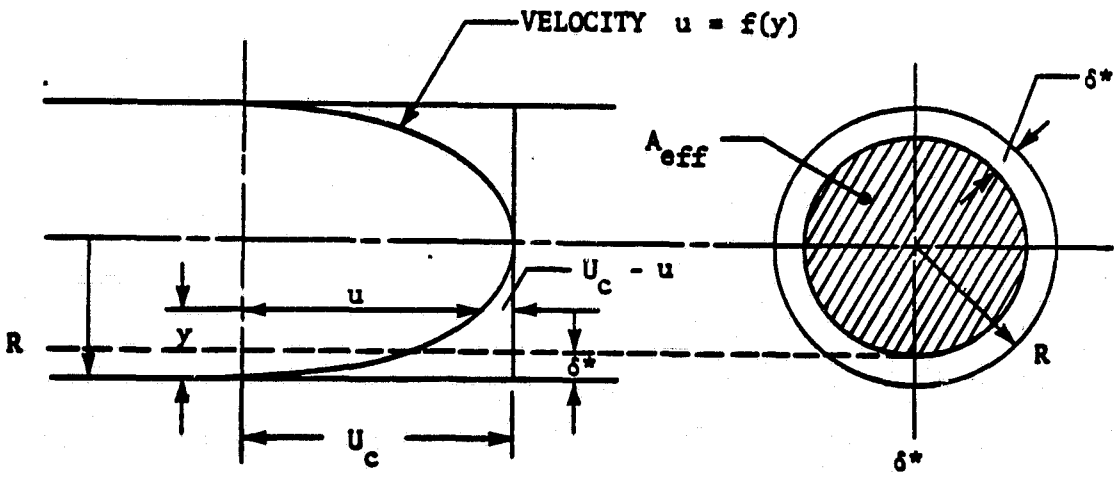

Figure B1.

REFERENCES

1. Barna, P.S.: Scale Model Studies for the Improvement of Flow Patterns of a Low-Speed Tunnel. Progress Report for NASA grant NSG 1563, Mar. 1981.

2. Barna, P.S.: Experimental Investigations on the V/STOL Tunnel at NASA/ Langley Research Center. NASA Contractor report 165655, Feb. 1981.

3. Barna, P.S.: Experiments with Tandem Diffusers with Boundary-Layer Suction Applied in Between. Final Report for NASA Contract NAS1-14193, Task Nos. 6 & 42, Aug. 1978.

4. Runstadler, P.W.; Dolan, F.X.; and Dean, R.C.: Diffuser Data Book. Creare Inc., Science and Technology (Hanover, New Hampshire), TN-186, May 1975.

5. Barna, P.S.: Fluid Mechanics for Engineers. Butterworth Ltd. (London), Third Edition, (S.I. Version), 1971, pp. 341-351.

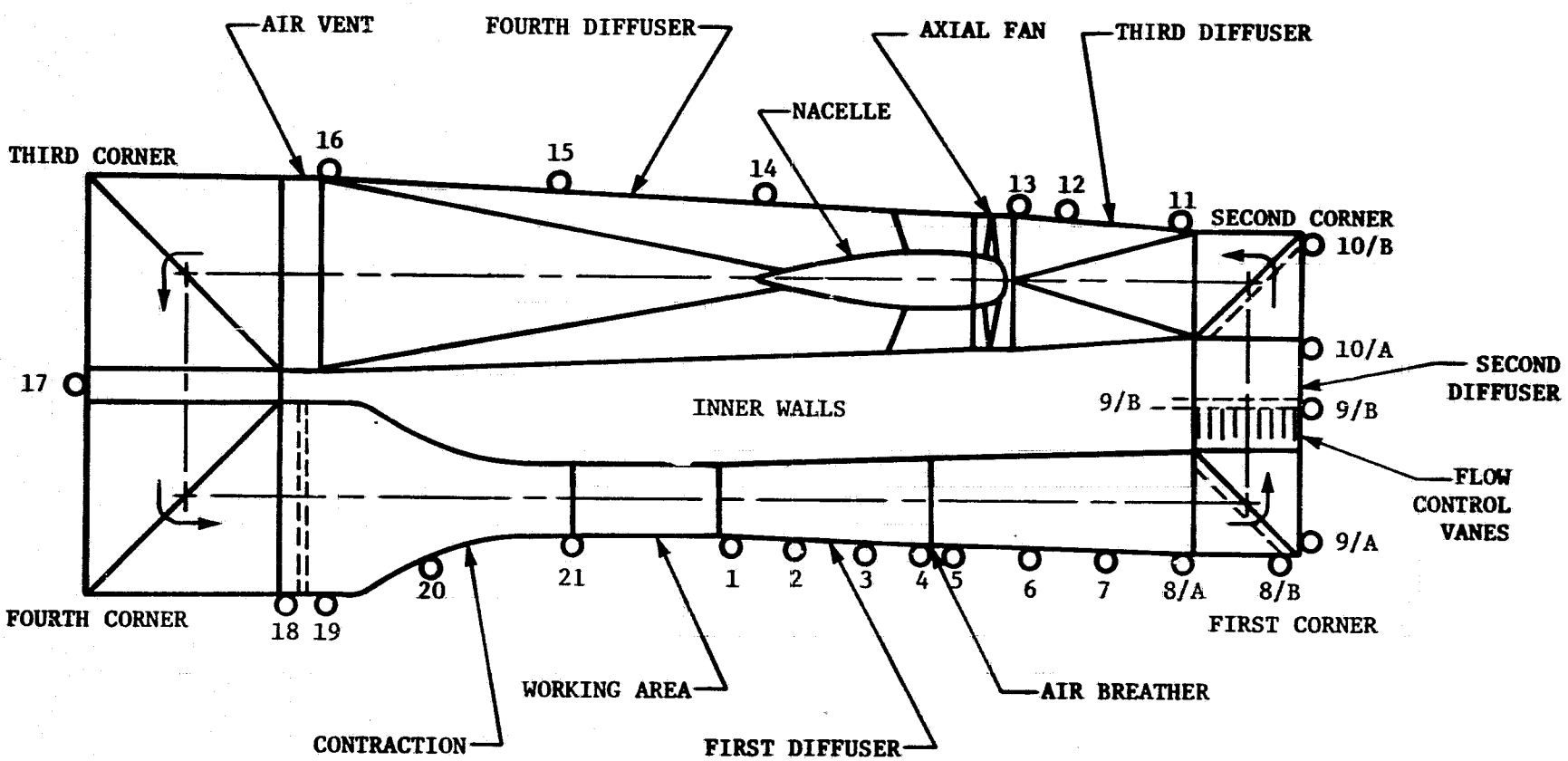

Figure 1(a). Plan view of the V/STOL tunnel. (Numbers 1 to 21 refer to traverse stations.)

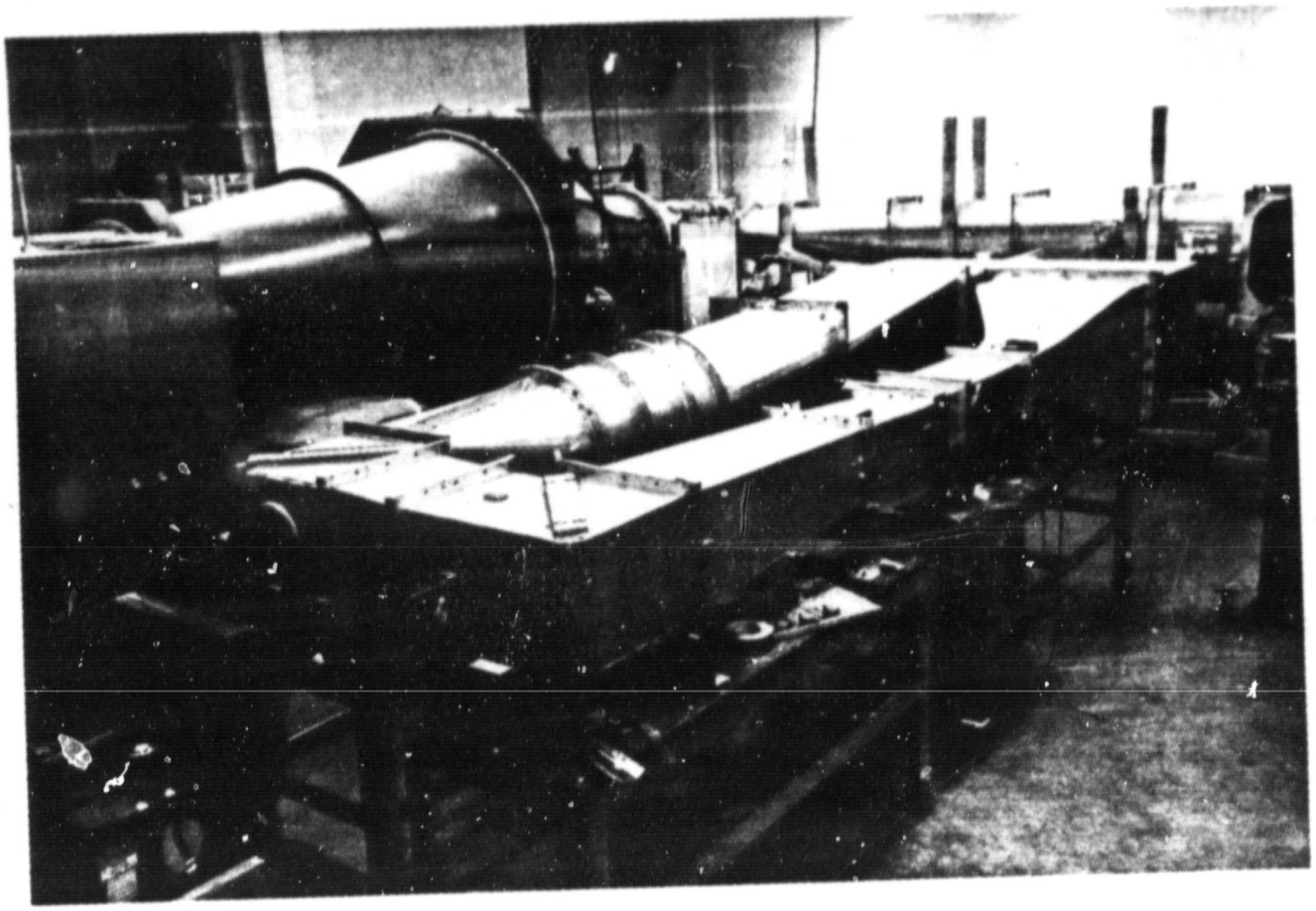

Figure 1(b). Photograph of the V/STOL tunnel.

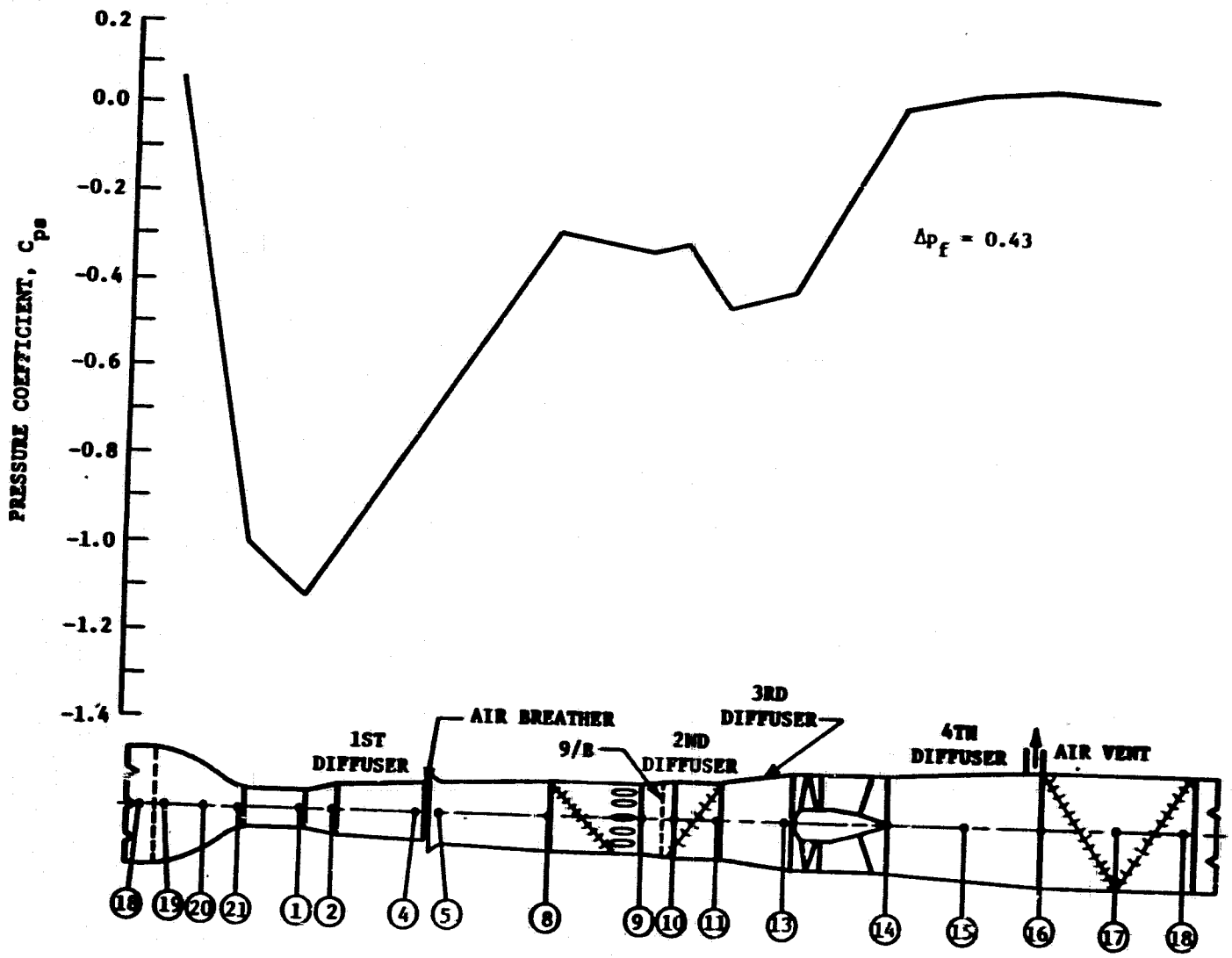

(a) Air breather closed

Figure 2. Pressure variation around V/STOL model tunnel circuit with a screen at TS 9/B, $\blacksquare = 42$, $\beta = 0.059$.

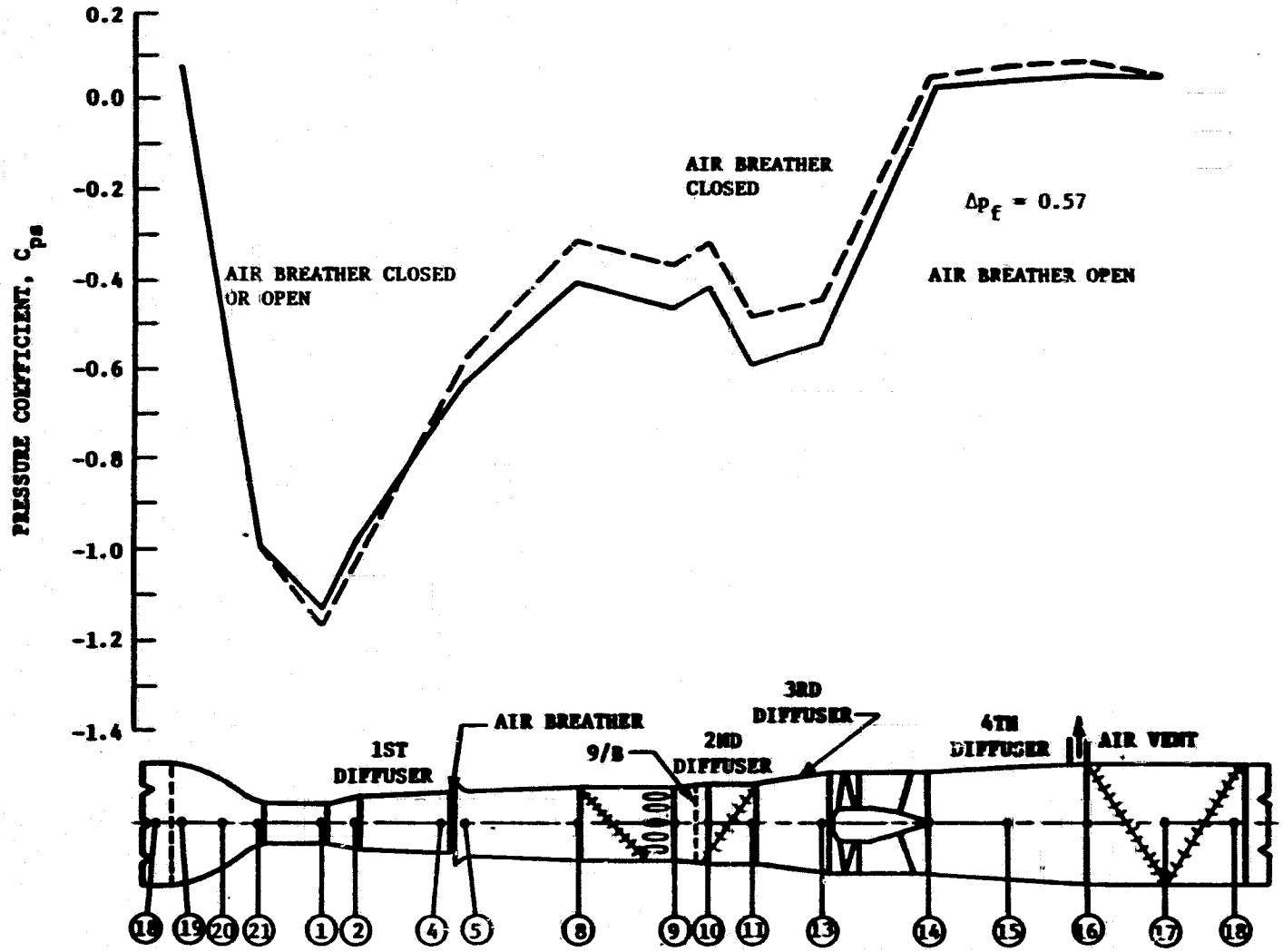

(b) Comparison of air breather open with air breather closed

Figure 2. (Concluded.)

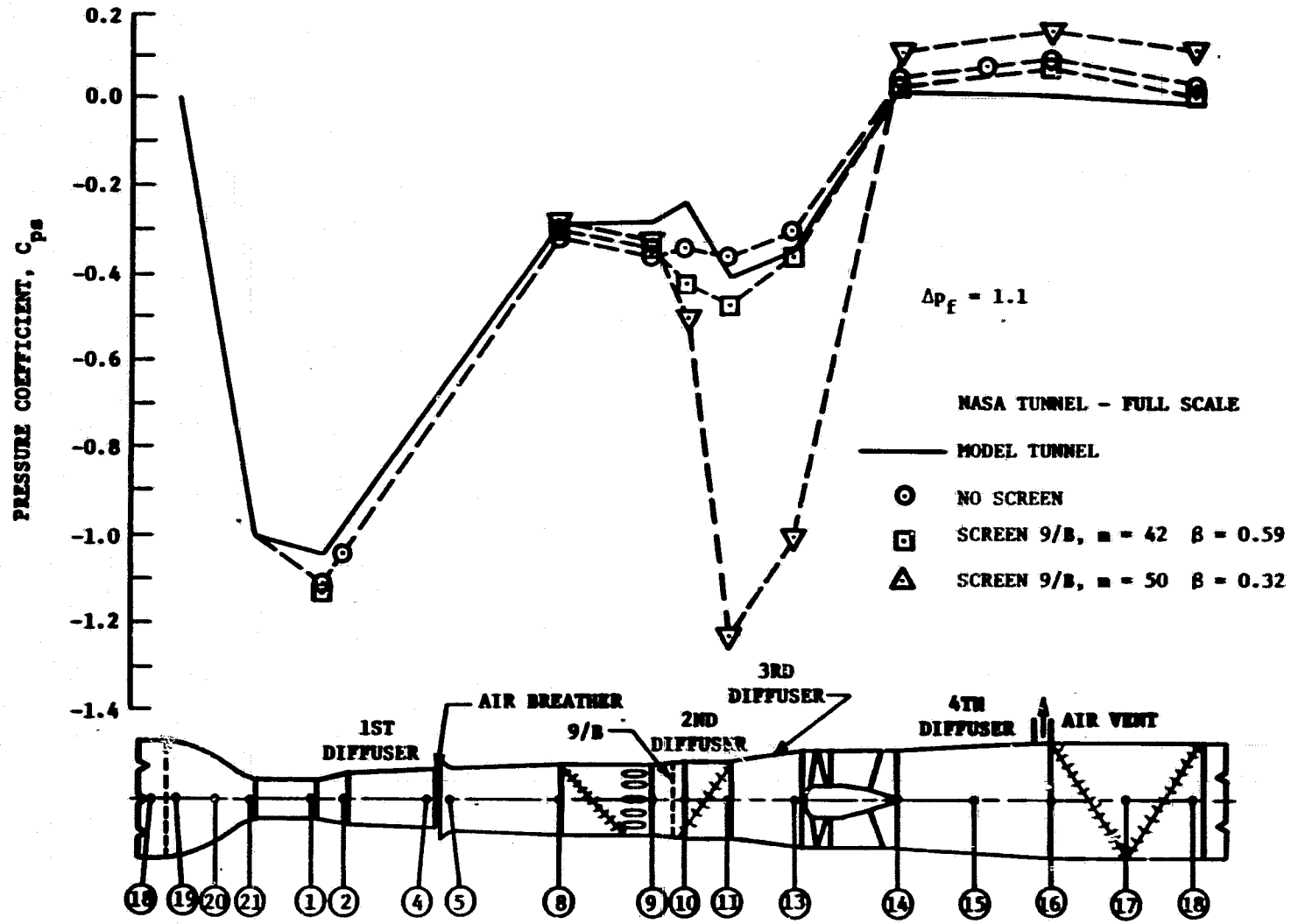

Figure 3. Comparison of pressure variations around model tunnel as affected by various screens.

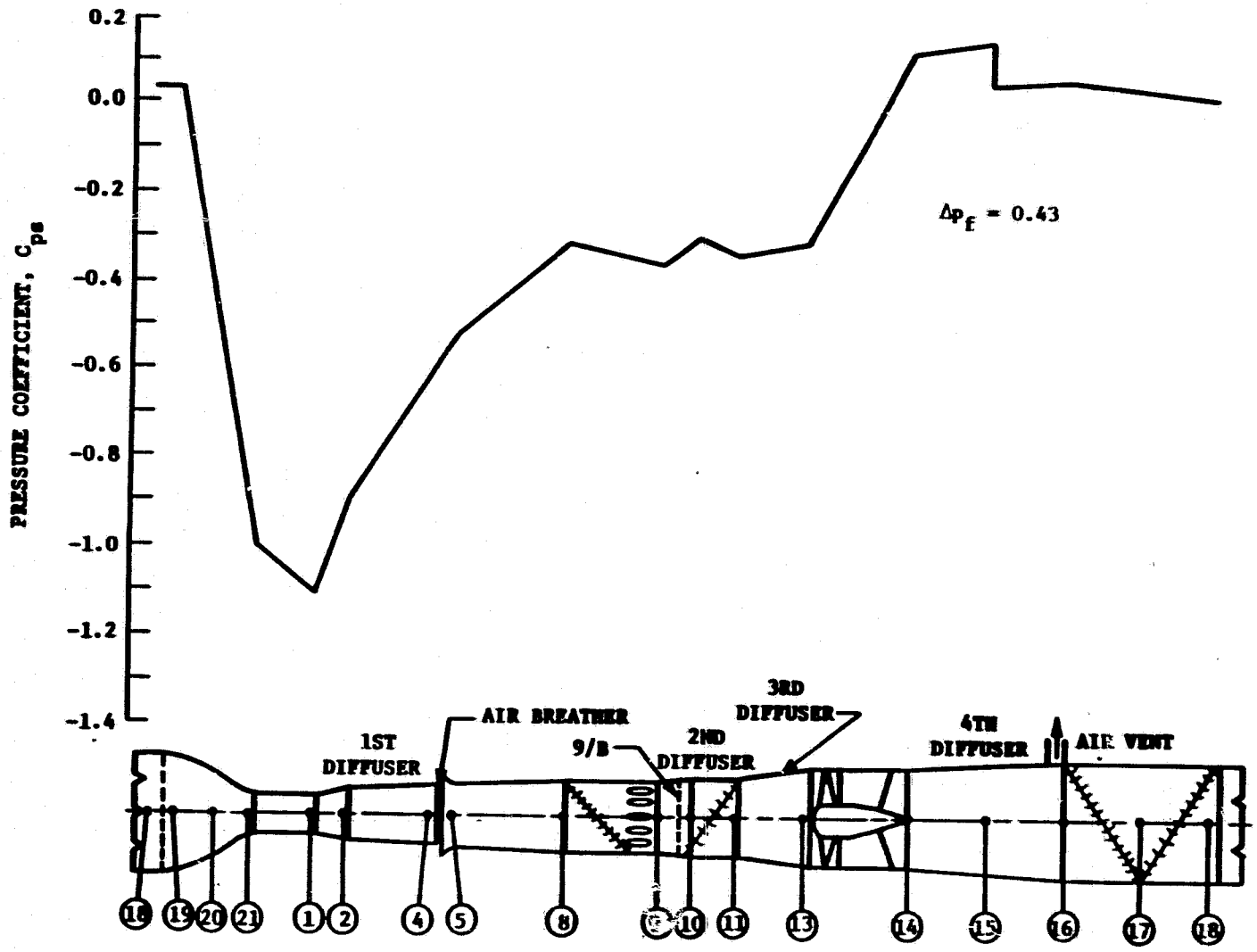

(a) No screen at TS 9/B; screen at TS 15, $m = 24$, $\beta = 0.57$

Figure 4. Pressure variation around model tunnel circuit with air breather closed--as affected by application of screens at traverse stations 9/B and 15.

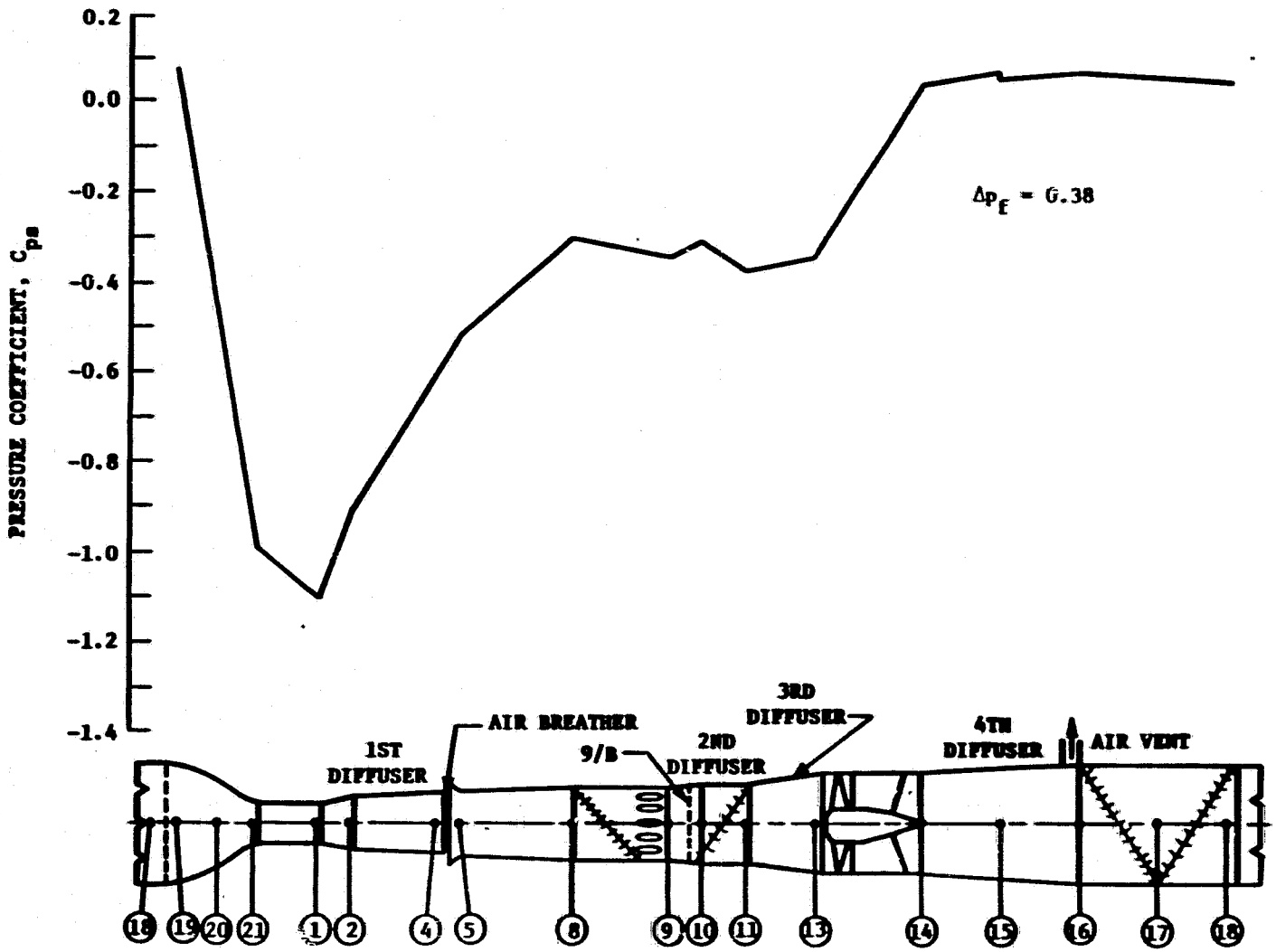

(b) Screen 1 at TS 9/B, m = 4, β = 0.83;
Screen 2 at TS 15, m = 16, β = 0.73

Figure 4. (Concluded).

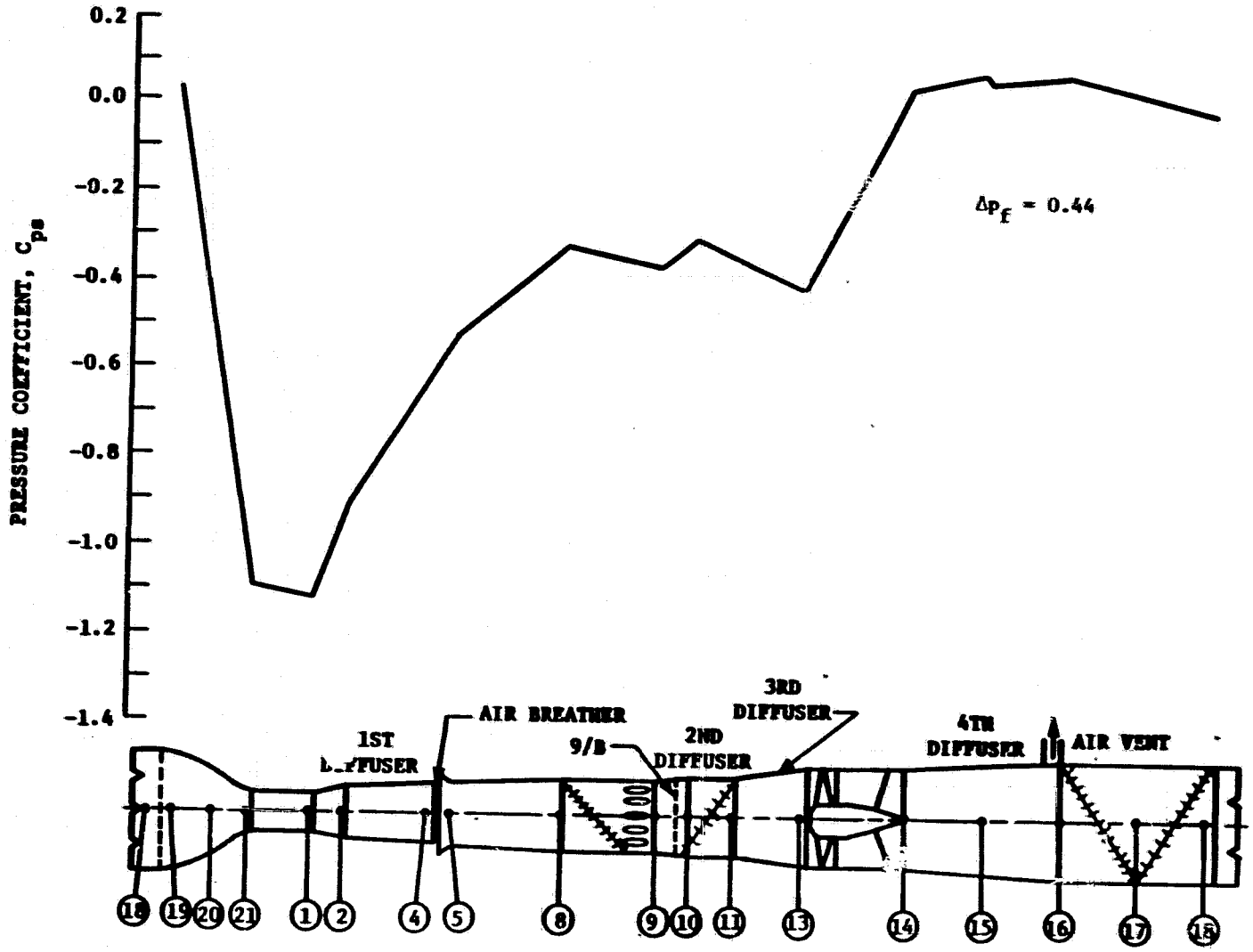

Figure 5. Pressure variation around model tunnel circuit with air breather closed--as affected by the presence of an orifice with a 45.7-cm (18-in.) opening at TS 12.

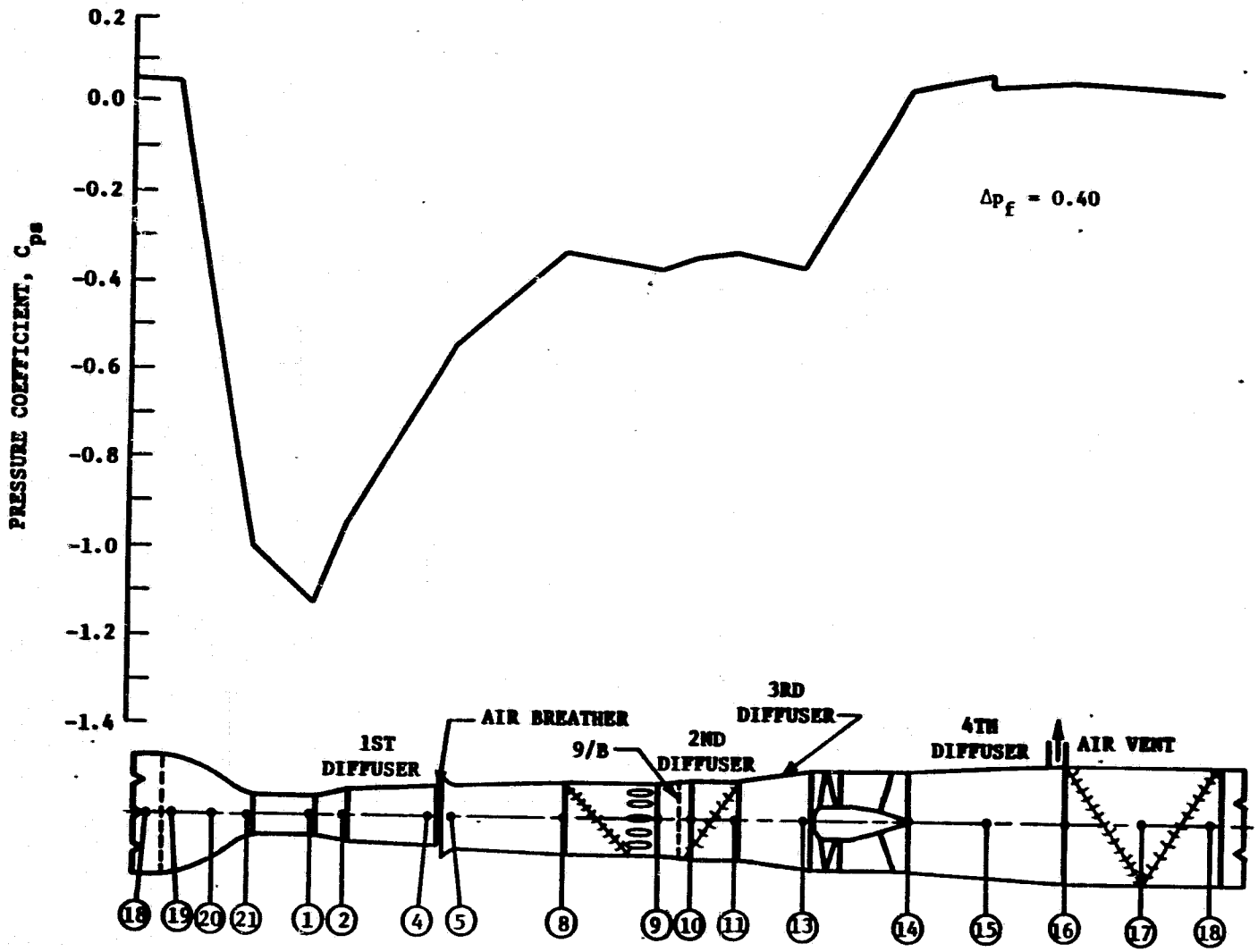

Figure 6. Pressure variation around model tunnel circuit--as affected by no screen at TS 9/B and dual porosity screen at TS 15.

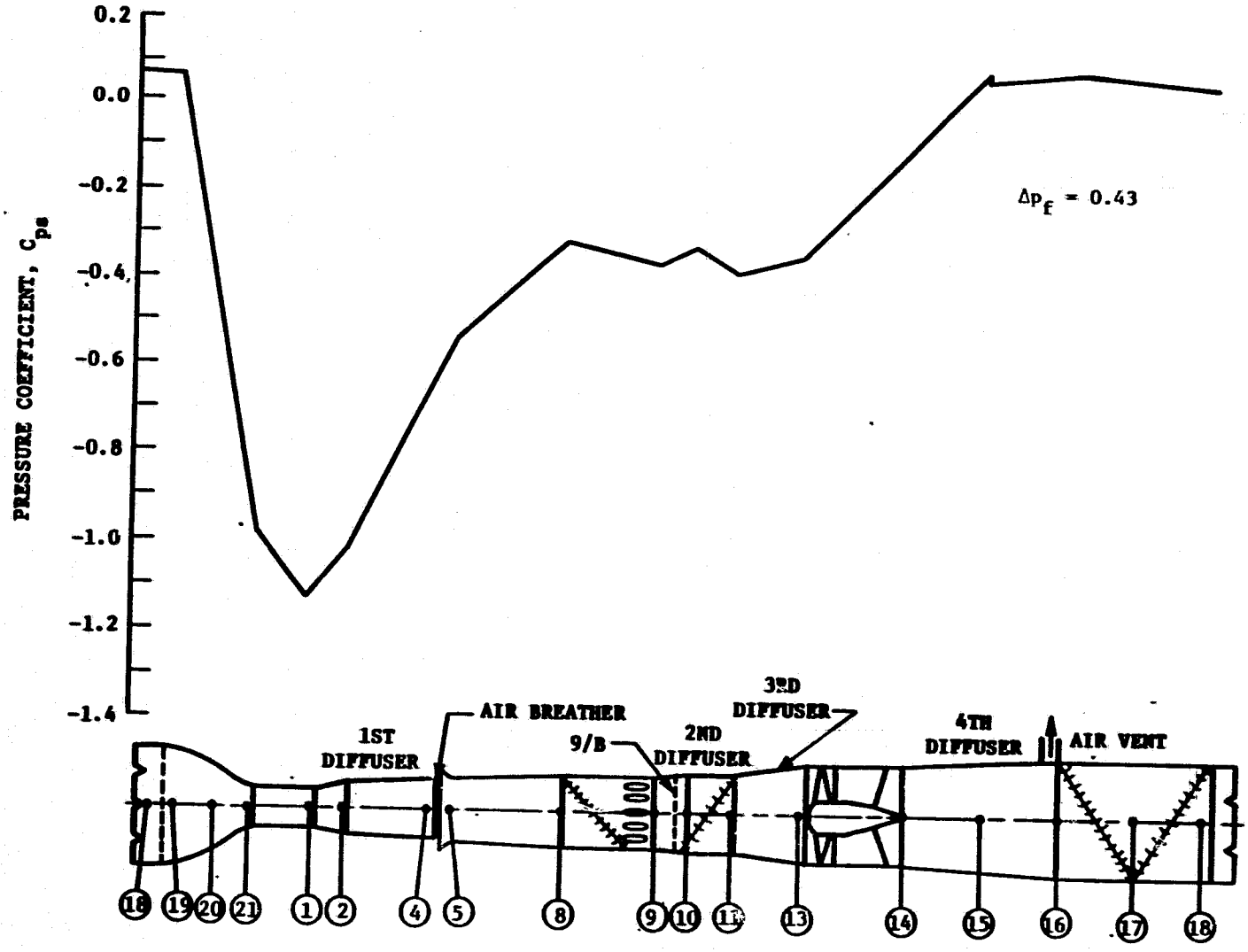

Figure 7. Pressure variation around model tunnel circuit--as affected by a screen at TS 9/B (m = 4, β = 0.83) and a multi-tier screen at TS 15.

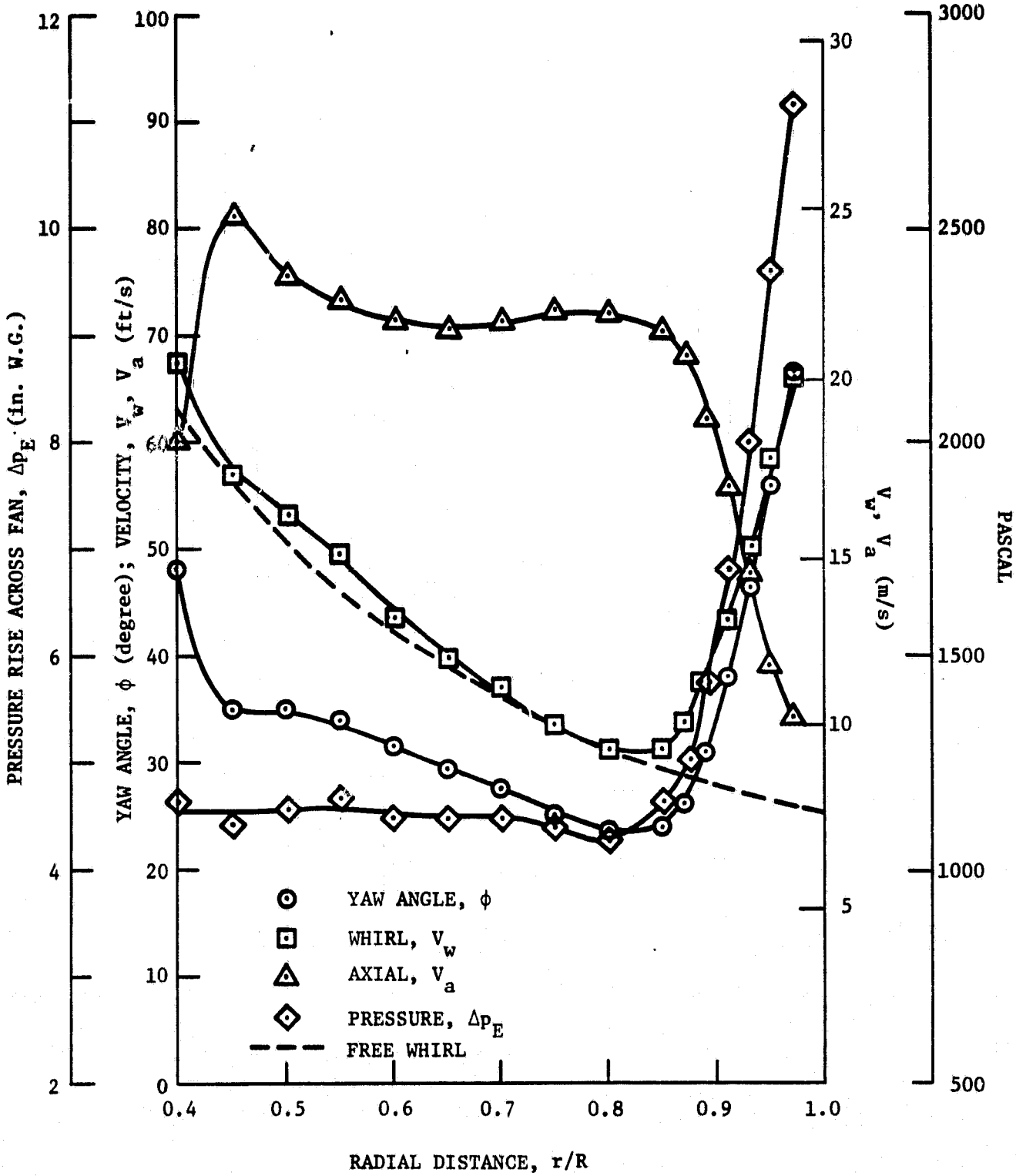

Figure 8. Variation of fan performance along blade in absence of orifice and screens.

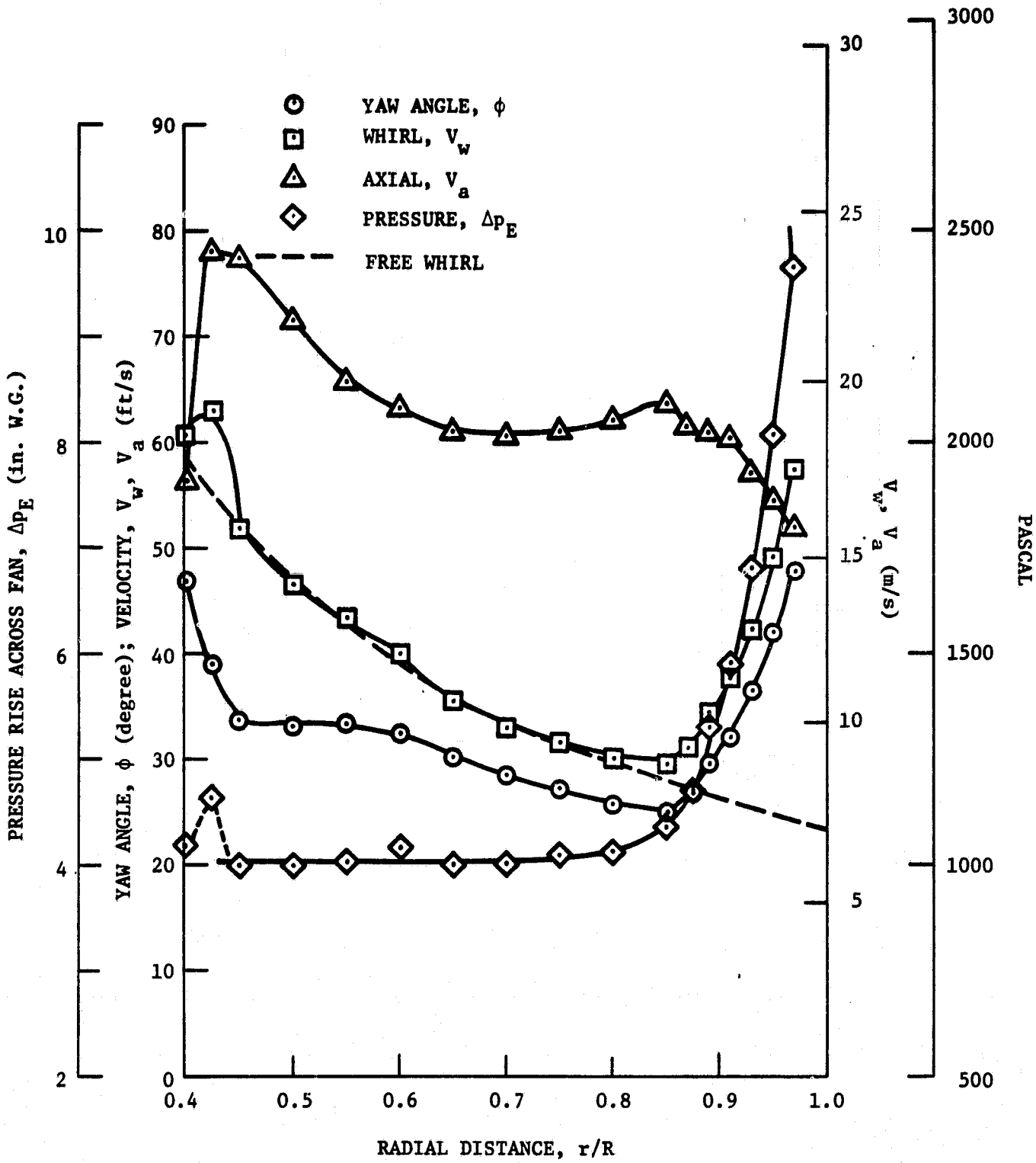

(b) Orifice size 45.72 cm (18 in.)

Figure 9. (Continued.)

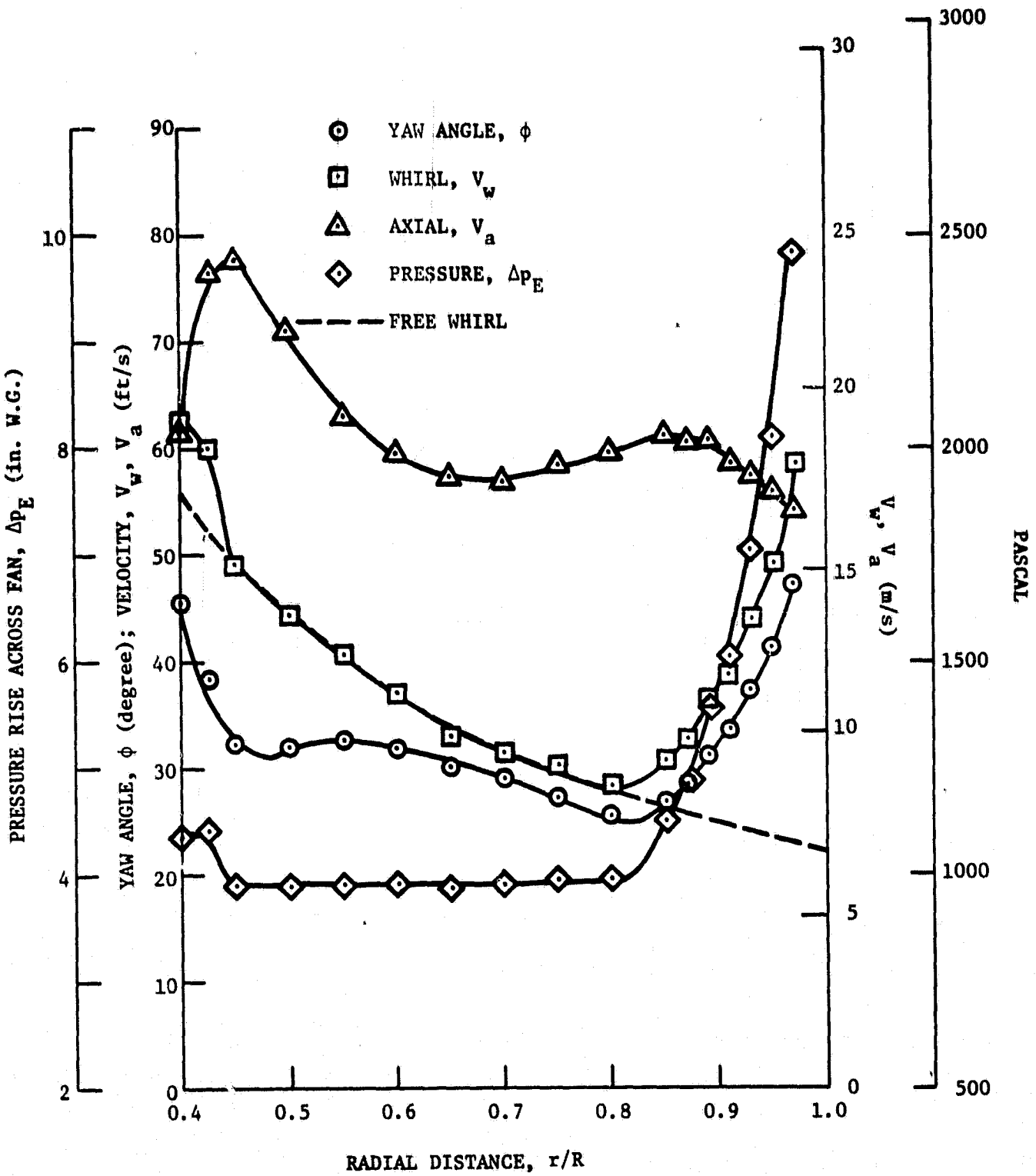

(c) Orifice size 43.18 cm (17 in.)

Figure 9. (Concluded.)

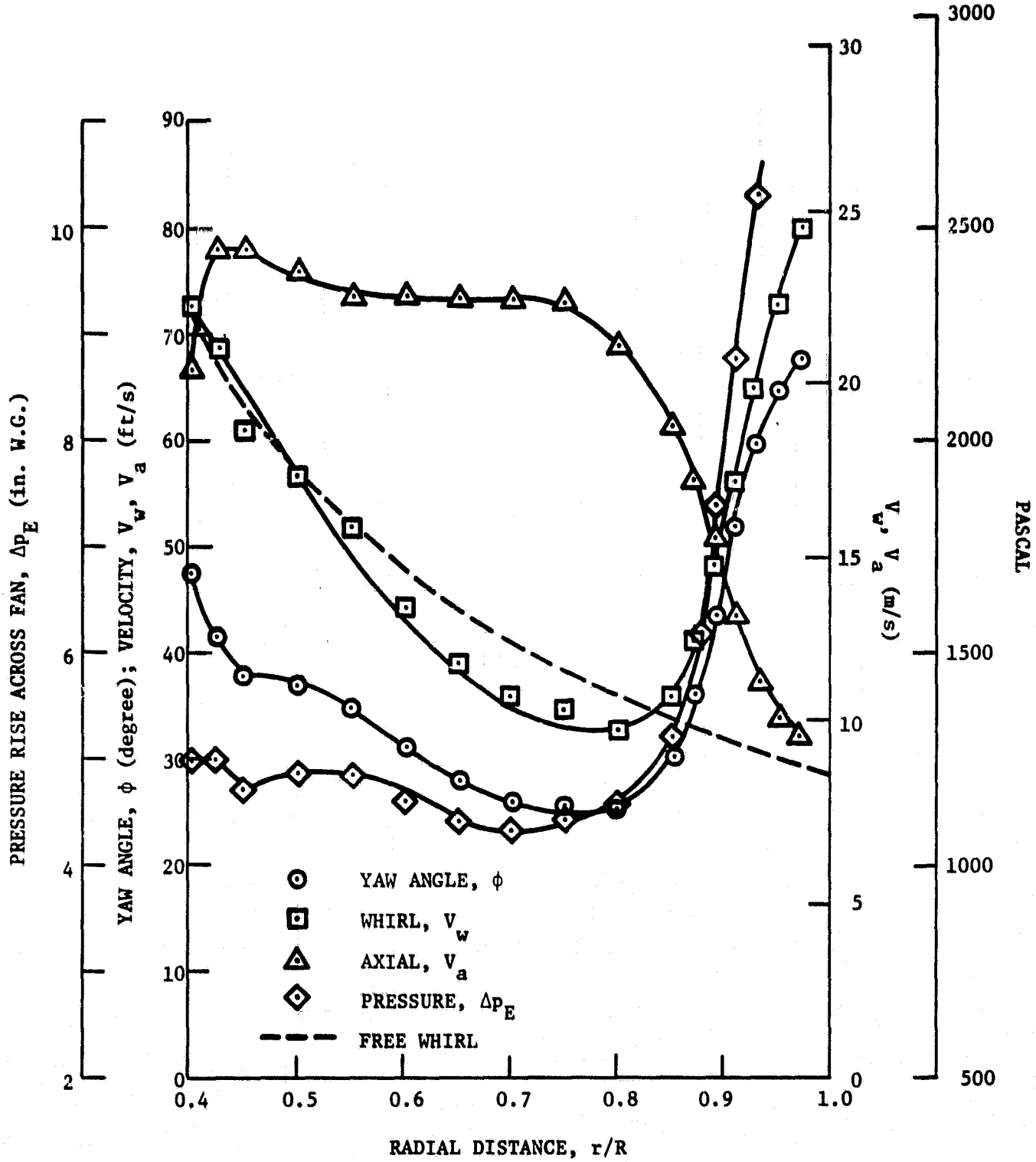

(a) No orifice; screen at TS 9/B, m = 42, β = 0.59

Figure 10. Variation of fan performance along blade with increasing screen resistance.

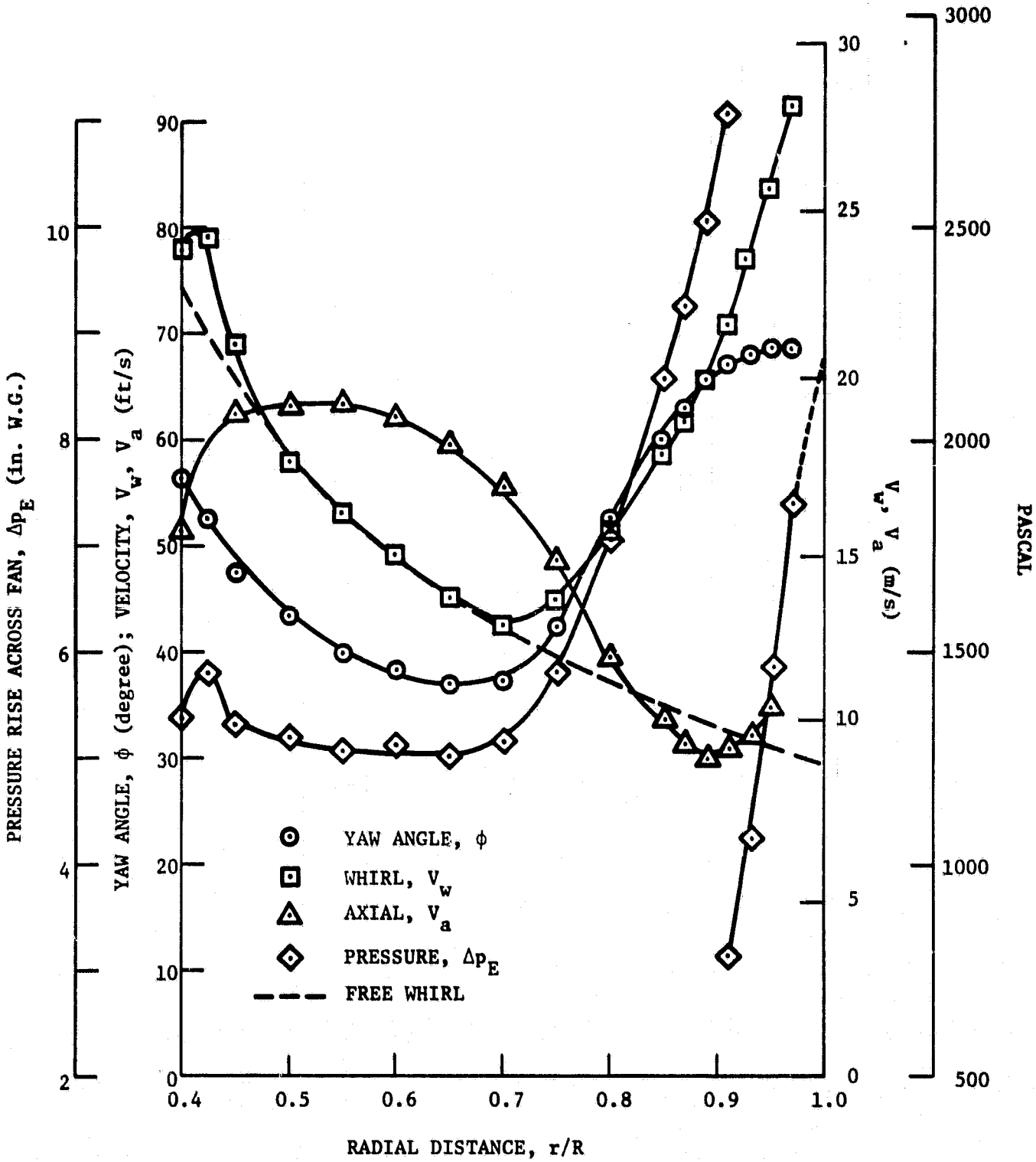

(b) No orifice; screen at TS 9/B, m = 50, β = 0.32

Figure 10. (Concluded.)

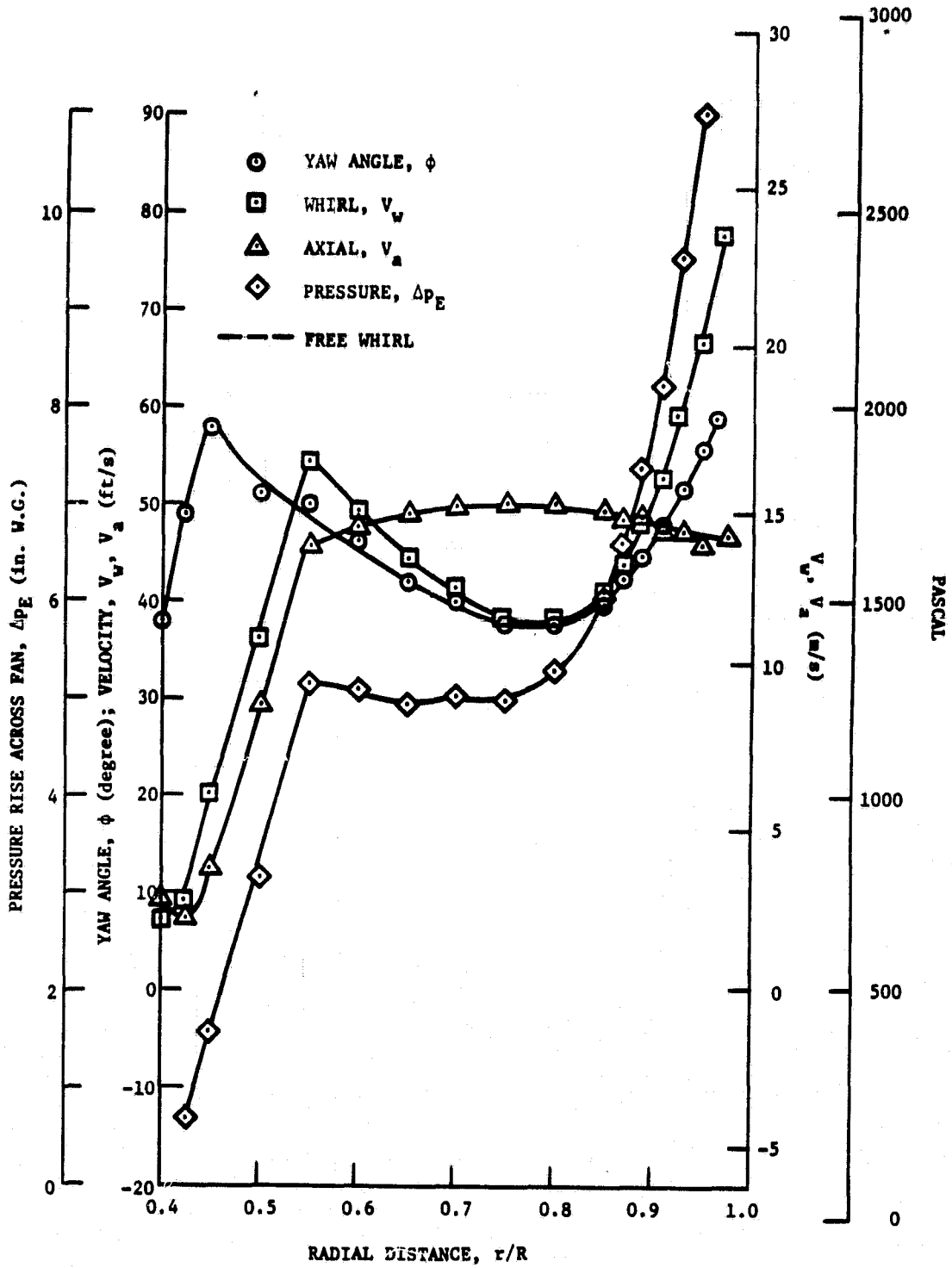

Figure 11. Variation of fan performance along blade in presence of an orifice and screen; orifice 43.18 cm (17 in.), screen at TS 9/B, m = 50, β = 0.32.

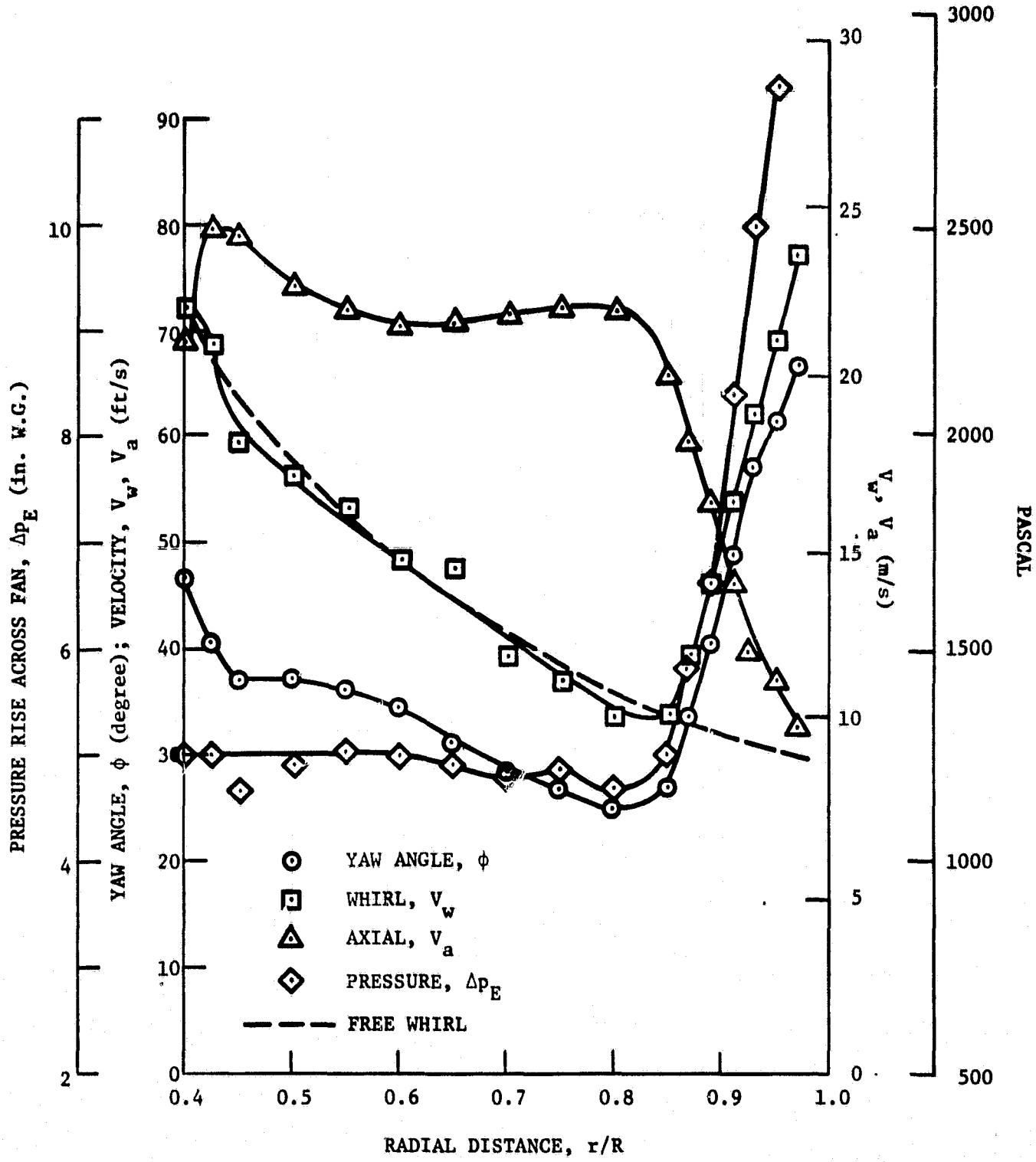

Figure 12. Variation of fan performance along blade in absence of orifice and screen at TS 9/B; screen only at TS 15, m = 24, β = 0.57.

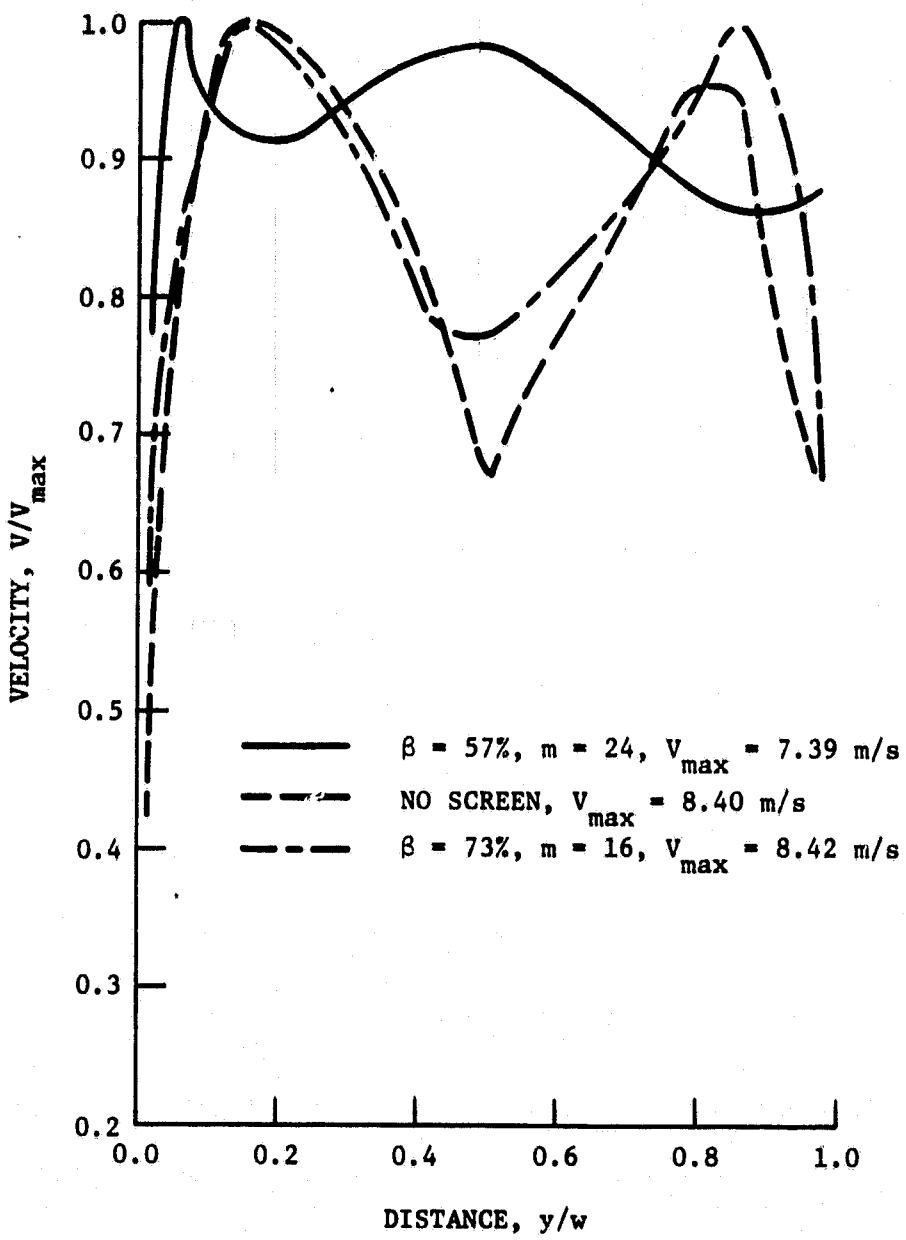

Figure 13. The effects of a single screen located at TS 15 on the downstream flow observed at TS 16 with 45.7-cm (18-in.) orifice at TS 13; screen: m = 24, β = 0.57.

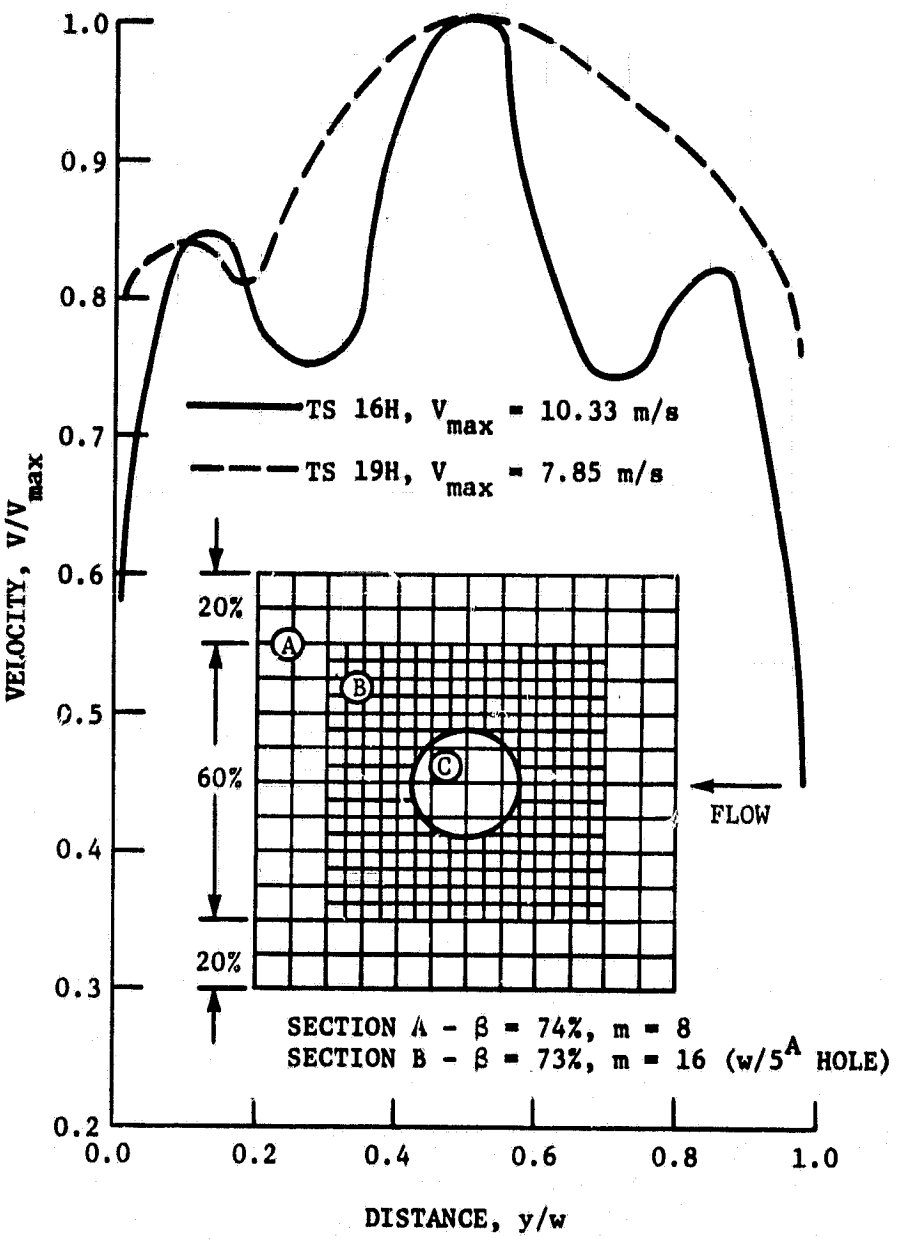

Figure 14. Effects of a multi-tier screen located at TS 15 on the downstream flow observed at traverse stations 16 and 19.

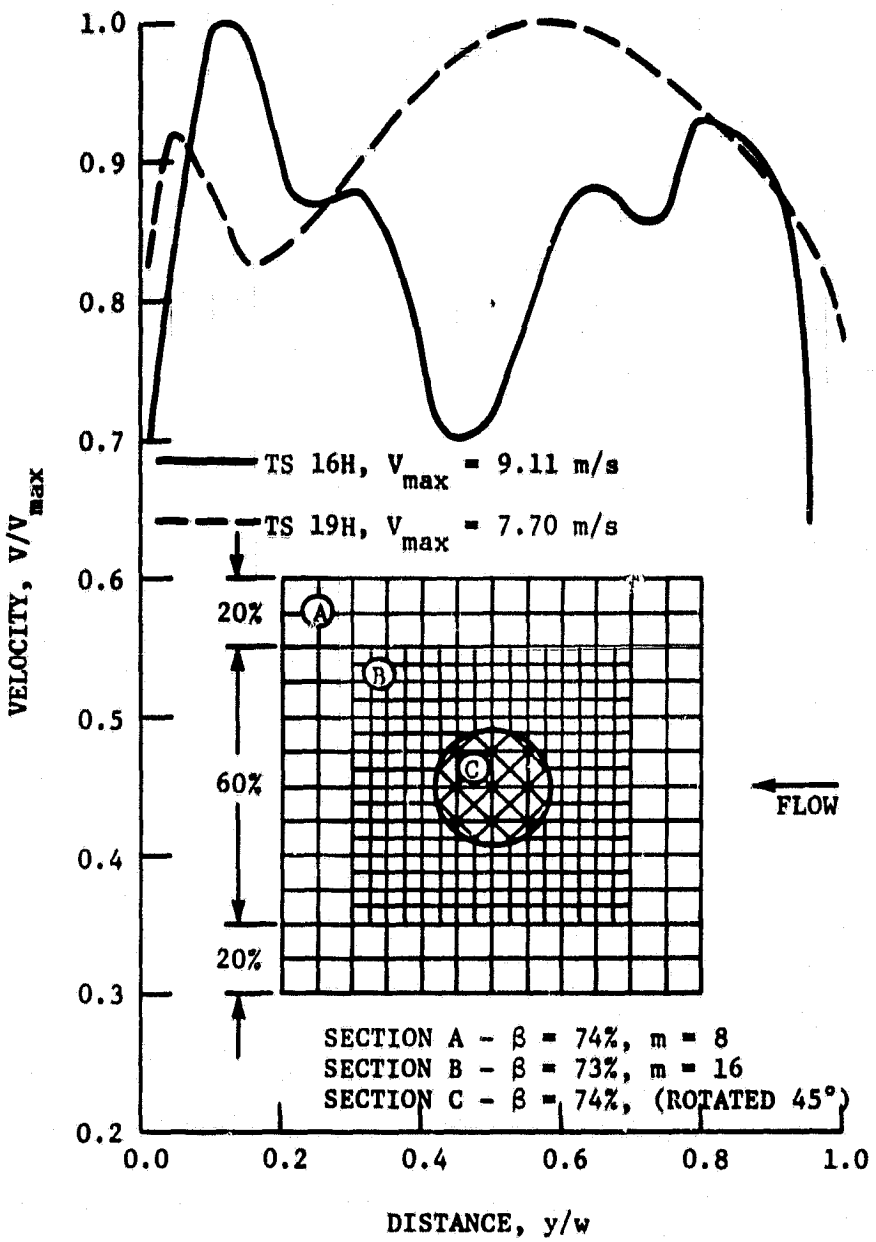

(b) Composite B

Figure 14. (Continued.)

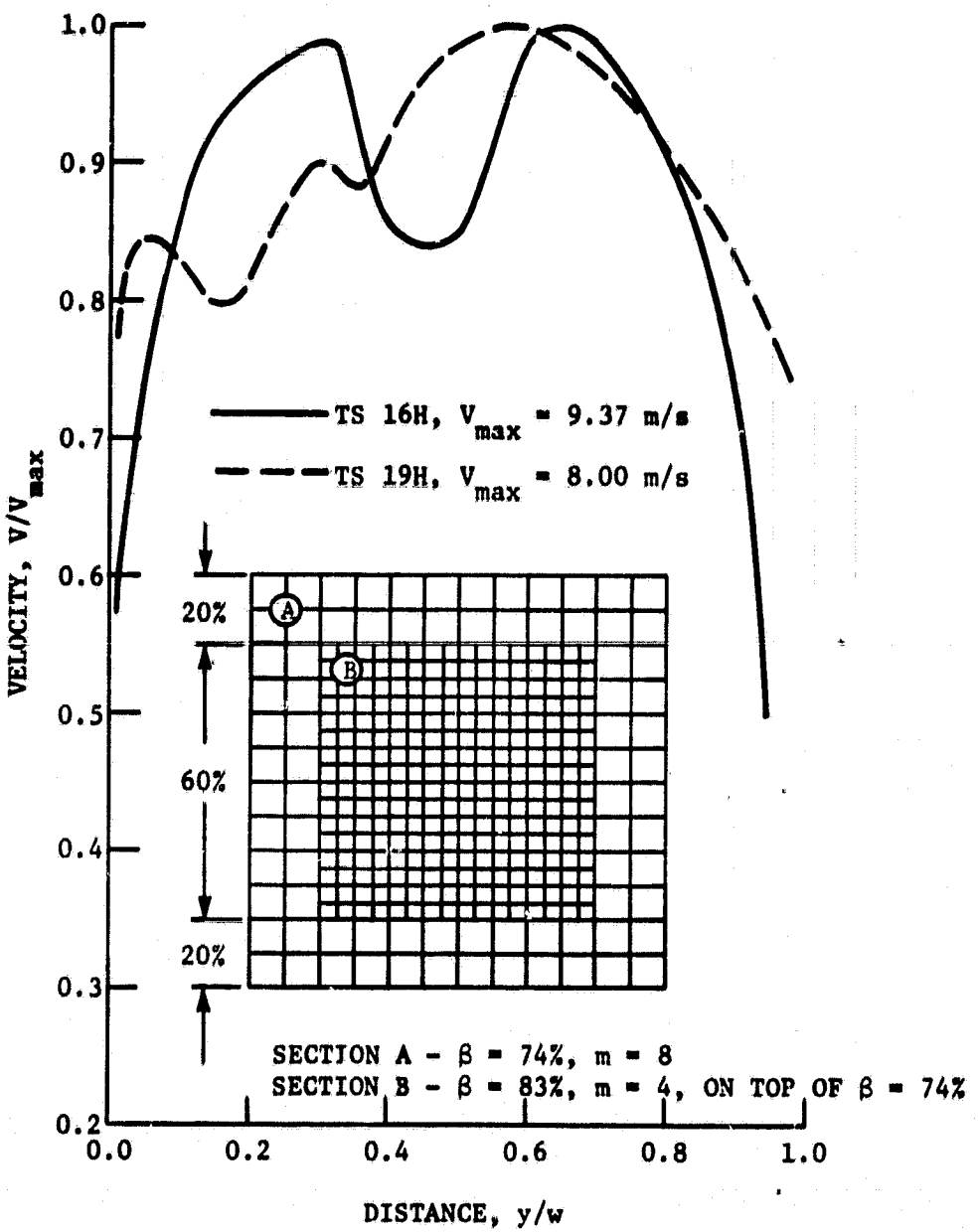

(c) Composite C

Figure 14. (Continued.)

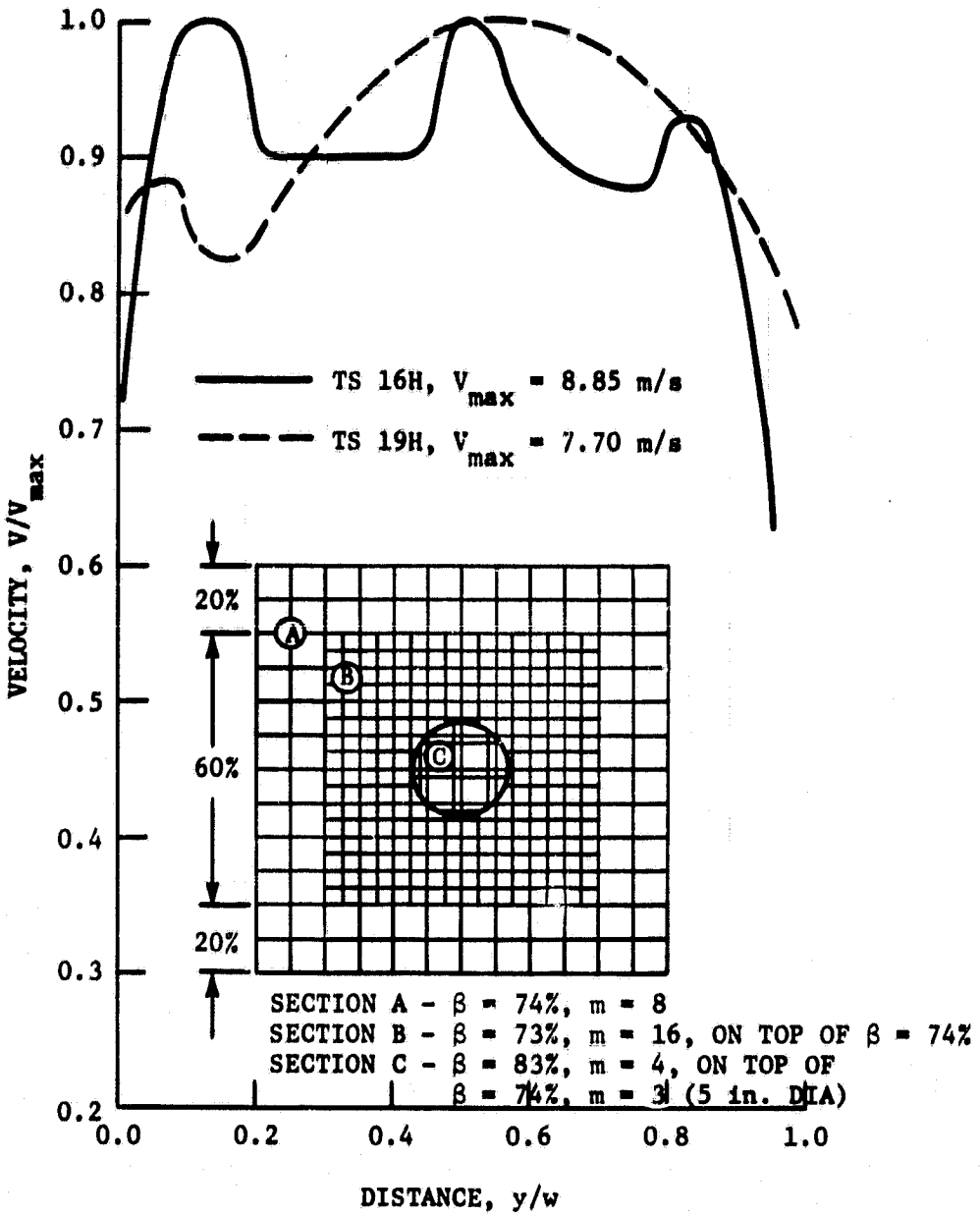

(d) Composite D

Figure 14. (Continued.)

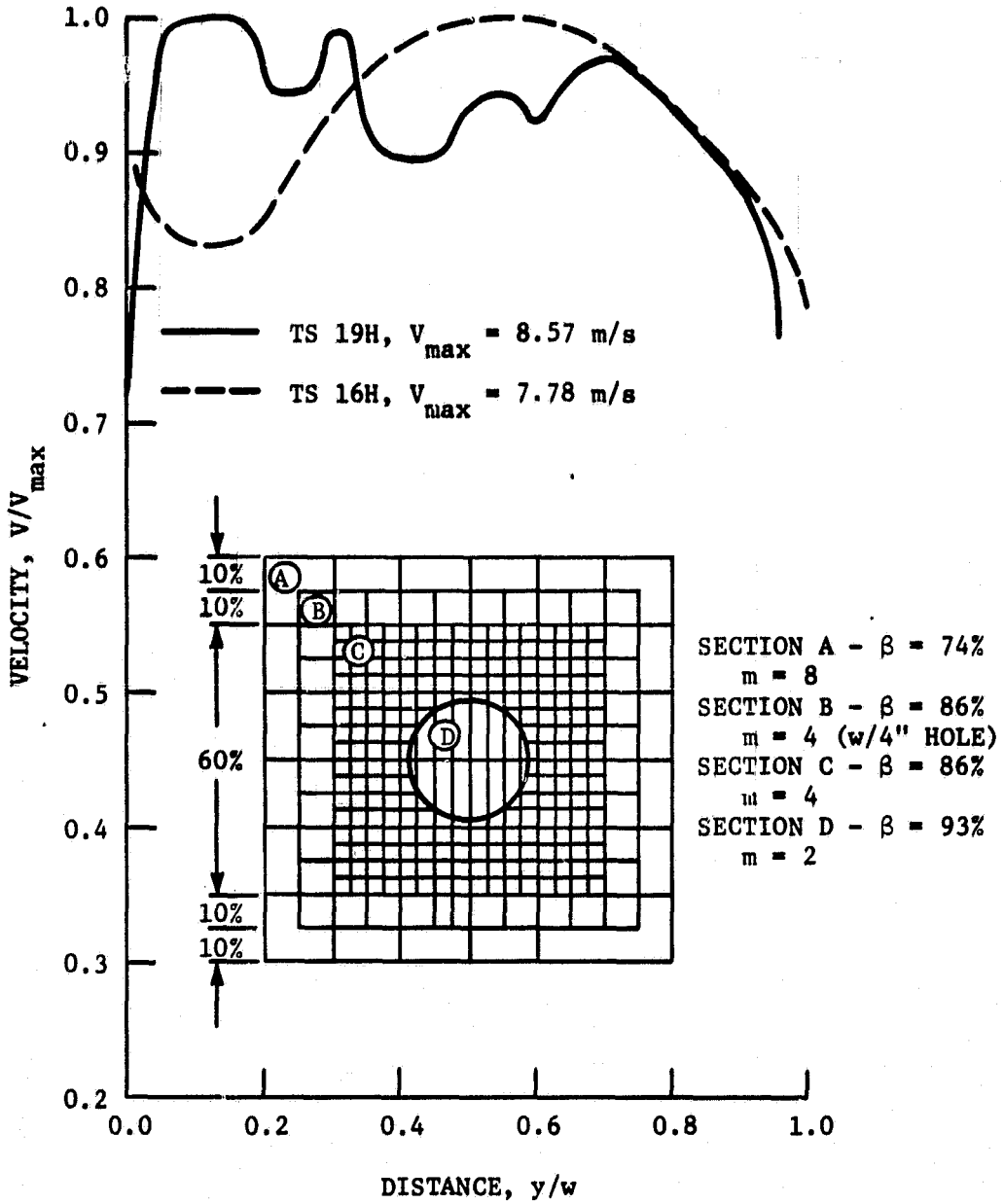

(e) Composite E

Figure 14. (Concluded).

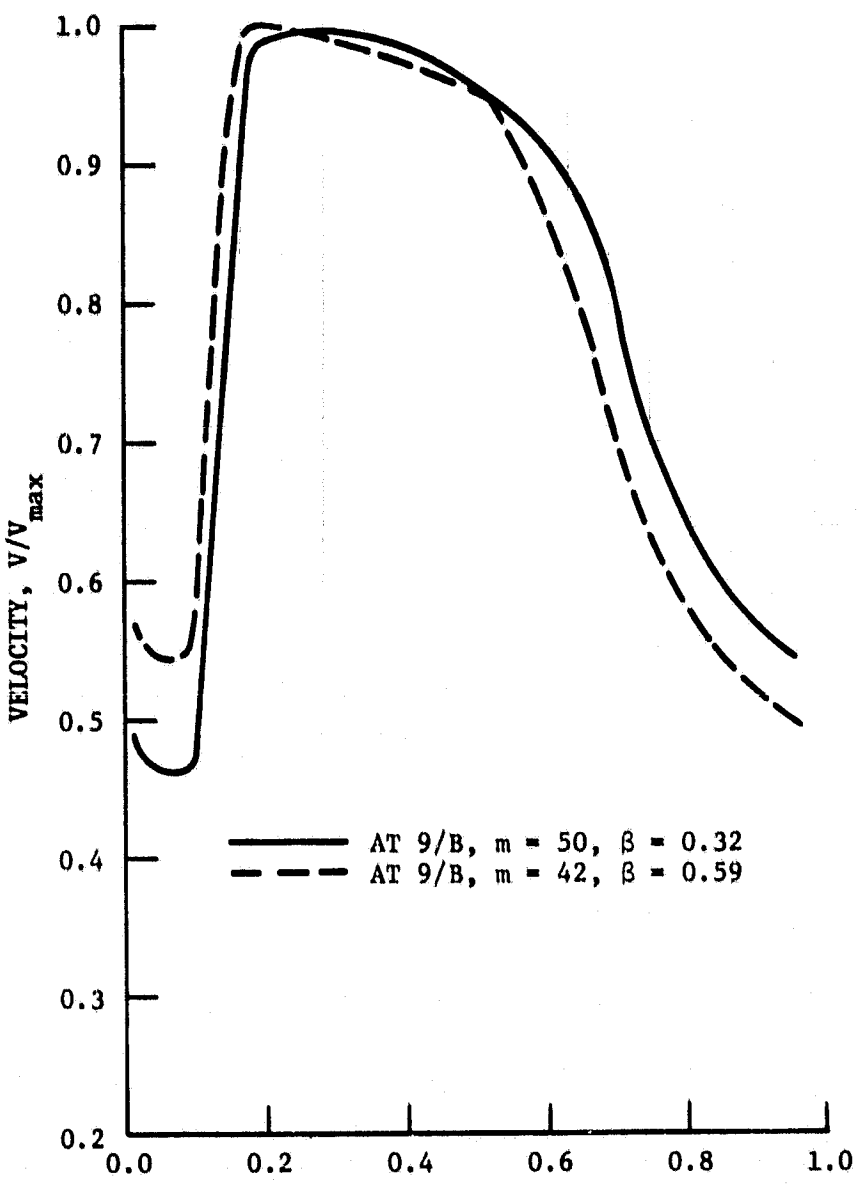

Figure 15. The upstream effects of a screen on the velocity distribution in the horizontal plane at TS 9/B.

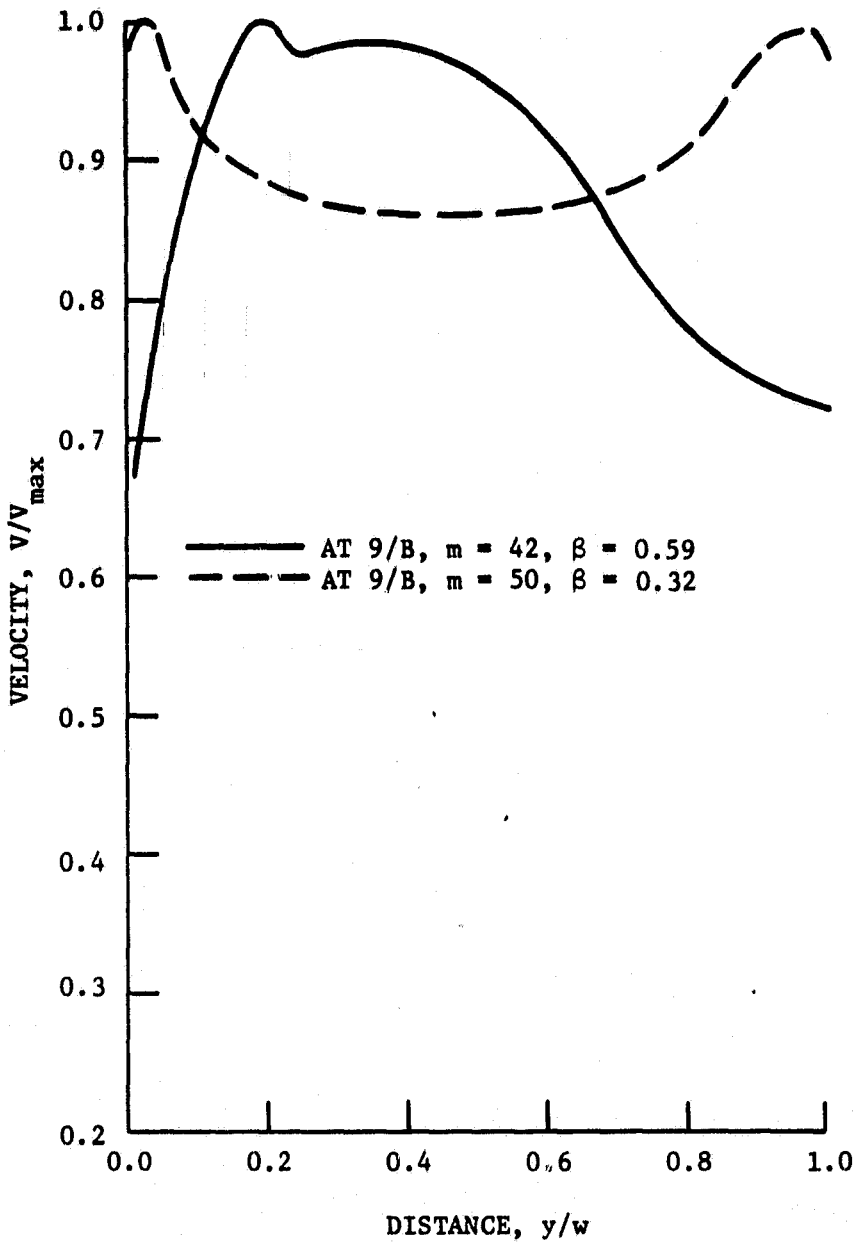

Figure 16. The downstream effects of a screen on the velocity distribution in the horizontal plane at TS 10/A.

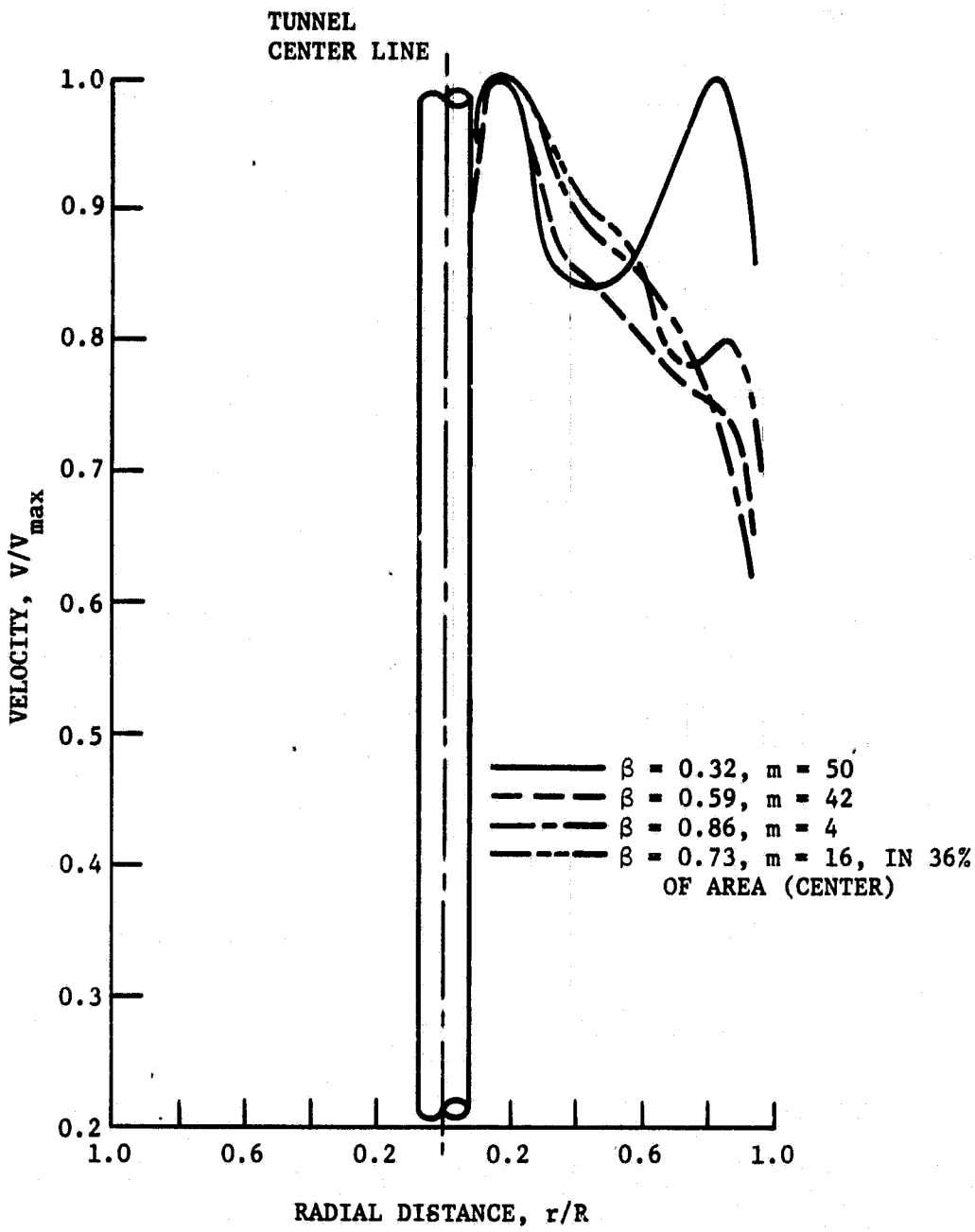

Figure 17. Velocity distribution immediately upstream from the fan at TS 13--as affected by application of various screens at TS 9/B.